# A novel leucine-rich repeat receptor-like kinase facilitates plant defense against *Fusarium oxysporum* infection

Hsin-Yao Huang[1*], Juan Carlos Montesinos[1*], Gloria Sancho-Andrés[1], Apolonio Ignacio Huerta[1], Anurag Kashyap[2], Huanjie Yang[3], Nuria S. Coll[2], Cyril Zipfel[3], Clara Sánchez-Rodríguez[1†]

[1]Institute of Molecular Plant Biology, Department of Biology, ETH Zürich, Zürich, Switzerland

[2]Centre for Research in Agricultural Genomics (CRAG), CSIC-IRTA-UAB-UB, Barcelona, Spain

[3]Institute of Plant and Microbial Biology, Zurich-Basel Plant Science Center, University of Zurich, Zurich, Switzerland

[*]Equal contribution

[†]Corresponding author: clara_sanchez@ethz.ch

**Abstract**

Plant cell walls are complex and dynamic polysaccharide networks that act as the first physical barrier of the cells and provide them structural support. Therefore, the maintenance of cell wall integrity is vital for growth and adaptation to a constantly changing environment. Cell wall integrity can be altered by numerous environmental stresses, including biotic stresses. Pathogens like *Fusarium oxysporum* (Fo), a soil-borne fungus widespread around the world, have significant impact on cell wall integrity during their infection. Fo infects the plant roots by penetrating in between root epidermal cells. Its hyphae later travel through this extracellular space in roots called apoplast, which mainly comprises plant cell walls, towards root vasculature. During its movement in the apoplast, Fo secretes plenty of cell wall modifying proteins to loosen and degrade the plant cell wall and facilitate the fungal infection. It is important that plant cells recognize these changes in their cell walls and trigger the responses to halt Fo infection. This process is achieved through, among others, plasma membrane-localized sensor proteins, whose turnover is controlled by endomembrane trafficking. In this study, we identified the leucine-rich repeat receptor-like kinase MEE39 as a plasma membrane receptor involved in plant defense against Fo. Furthermore, MEE39 was found to be required for sensitivity to isoxaben (ISX) induced cellulose synthesis inhibition. *MEE39* transcription was activated by Fo and ISX treatments. However, its protein accumulation was decreased by Fo while enhanced by ISX treatment. A previously reported cell wall integrity sensor, MIK2, was discovered as a potential interactor of MEE39 functioning in the MEE39-dependent plant defense against Fo. Taken together, we found a new plasma membrane player, MEE39, which seems to contribute to root defense and coordinate with sensing the cellulose synthesis inhibition induced by Fo infection.

## Introduction

The plant cell wall is a protective barrier of cells and the source of elicitors that trigger plant responses to environmental challenges (Lionetti & Métraux, 2014). Among the cell types that form a plant, epidermal cells equipped with the primary cell wall comprise the outmost layer of the plant. The primary cell wall is a flexible matrix composed of cellulose, hemicellulose, pectin, and cell wall remodeling proteins (Cosgrove, 2005), which supports plant growth and development while protecting plants from abiotic and biotic stresses. Cell wall integrity is constantly monitored by many sensors at plasma membrane (PM). Many of these sensors are receptors belonging to *Catharanthus roseus* receptor-like kinase1-like (CrRLK1L) subfamily, wall-associated kinase (WAK) family, and leucine-rich repeat receptor-like kinase (LRR-RLK) family (Wolf, 2017; Rui & Dinneny, 2020). CrRLK1Ls are characterized by two extracellular malectin-like domains. These domains share homology with the malectin protein that was originally found in *Xenopus laevis* cells (Schallus *et al*., 2008). Malectin was shown to share similar structure with the carbohydrate-binding modules from glycosyl transferases and interact with di-glucose motifs of N-linked oligoglycans (Schallus *et al*., 2008). However, evidence supporting CrRLK1Ls binding to carbohydrates to monitor cell wall integrity is scarce. The CrRLK1L THESEUS1 (THE1) was shown to be required for sensing genetically (*cesa6*$^{prc1\text{-}1}$; Hématy *et al*., 2007) and pharmacologically (Van der Does *et al*., 2017) induced cellulose synthesis inhibition without ligand identified. The best characterized CrRLK1L, FERONIA (FER) was shown to interact with the pectin component polygalacturonic acid (PGA) *in vitro* (Feng *et al*., 2018), but it remains to be clarified whether FER monitors cell wall integrity through this interaction. The WAK family are receptor-like kinases with extracellular domain binding to pectins and inducing cell wall signaling (Wagner & Kohorn, 2001). WAKs have been shown to bind to de-esterified homogalacturonan (HG), PGA, and HG-derived oligomers called oligogalacturonides (OGs) (Decreux & Messiaen, 2005; Decreux *et al*., 2006; Kohorn *et al*., 2009; Brutus *et al*., 2010). The perception of de-esterified HG activates downstream genes needed for cell expansion (Kohorn *et al*., 2009), and perception of OGs triggers immune responses (Brutus *et al*., 2010). LRR-RLKs, as the largest subgroup among RLKs, were not reported to interact with carbohydrates, despite that LRR-RLK I family possess the malectin-like domain (Wolf, 2017; Rui & Dinneny, 2020). Among LRR-RLKs, FEI1 and FEI2, are needed, under high sugar conditions, for cellulose synthesis and proper anisotropic cell expansion, in which the cell wall needs to be extended in a coordinate manner with turgor pressure and microtubule constraints (Xu *et al*., 2008). In addition, MALE DISCOVERER1-INTERACTING RECEPTOR LIKE KINASE2 (MIK2)

and STRUBBELIG (SUB) are LRR-RLKs suggested to sense cell wall integrity and regulate root growth when cellulose synthesis is pharmacologically inhibited (Van der Does *et al*., 2017; Chaudhary *et al*., 2020).

Some cell wall integrity sensors (or potential sensors), such as FER, THE1, WAK-LIKE 22 / RESISTANCE TO FUSARIUM OXYSPORUM 1 (RFO1), and LRR-RLK MALE DISCOVERER 1-INTERACTING RECEPTOR LIKE KINASE 2 (MIK2), have been shown to play a role in plant defense against an agronomically important fungal pathogen, *Fusarium oxysporum* (Fo; Diener & Ausubel, 2005; Masachis *et al*., 2016; Van der Does *et al*., 2017). Pathogenic Fo can infect more than 100 plant species, including important crops, for instance, banana, tomato, cotton, soybean, and cabbage (Michielse & Rep, 2009; Gordon, 2017; Edel-Hermann & Lecomte, 2019). The soil-borne Fo infects plants from the roots. In outer root cell layers (i.e. from epidermis to cortex), the fungus attaches to the root and the hyphae advances mainly intercellularly to approach the plant vasculature (De Coninck *et al*., 2015; Bani *et al*., 2018; Menna *et al*., 2021). After arriving in the xylem, the fungal proliferation blocks water transport and results in the wilting disease with yellow and dry leaves aboveground, which eventually causes plant death (Michielse & Rep, 2009). During the infection, Fo secretes cell wall-degrading enzymes such as cellulases, xylanases, and polygalacturonases (Kubicek *et al*., 2014) to facilitate its penetration through the root cell walls. Cellulose-derived cellobiose and pectin-derived OGs are hypothesized to be released from this cell wall degradation and act as damage-associated molecular patterns (DAMPs) activating plant defense signaling (Doares *et al*., 1995; de Azevedo Souza *et al*., 2017; Kesten *et al*., 2017). Recent works studying the *Arabidopsis thaliana*-Fo5176 model pathosystem have revealed that Fo also interrupts cell wall integrity by inducing the removal of cellulose synthase at the PM and downregulating cellulose synthesis genes, resulting in cellulose synthesis inhibition (Kesten *et al*., 2019; Menna *et al*., 2021). This cellulose synthesis inhibition may be sensed by the cell wall integrity sensors such as THE1 and MIK2. However, these are very few known cases of PM-localized cell wall sensors involved in plant response to Fo, and it is highly possible that more remain to be identified.

Receptors at the PM constantly undergo endocytosis to regulate their abundance and signaling at the PM (Schwihla & Korbei, 2020), and receptor endocytosis could be enhanced by ligand perception (Ben Khaled *et al*., 2015). Therefore, identifying and characterizing the receptor(s) that is/are internalized during Fo infection provide insight into understanding plant perception of this fungal pathogen. To identify such receptors, we analyzed the proteins immunoisolated from multivesicular body/prevacuolar compartment (MVB/PVC), which is the organelle to

receive cargos from the endocytic trafficking for vacuolar degradation (Robinson *et al*., 2008). An LRR-RLK I family member, MATERNAL EFFECT EMBRYO ARREST 39 (MEE39), was found to be enriched in MVB/PVC upon Fo infection. Our data indicated that MEE39 is PM-localized. Interestingly, *MEE39* expression was found to be heterogeneously expressed in root tissues, which is stronger in more differentiated tissues. Loss of MEE39 function resulted in reduced resistance to both *Fusarium* and *Ralstonia* wilt, and less sensitivity to isoxaben treatment. Furthermore, MIK2 was identified as a potential interactor of MEE39 contributing to the MEE39-dependent resistance to Fo vascular penetration. Our results suggest that MEE39 is a novel cell wall integrity sensor, which contributes to plant defense against wilting diseases.

**Results**

*MEE39 is identified as a plasma membrane-localized receptor-like protein needed for plant defense against wilting diseases*

After signal perception, PM receptors are internalized and trafficked through the MVB/PVC towards the vacuole for degradation (Fig. S1; Ben Khaled *et al*., 2015). Therefore, in order to identify new plant receptors involved in plant defense to Fo, we performed organelle immunoprecipitation (IP) using Fo5176-infected Arabidopsis roots expressing the MVB/PVC specific marker ARA7-YFP or free-GFP as a negative control. Plants were exposed to the Fo5176 microconidia and grown hydroponically as previously described (Menna *et al*., 2021), and roots were harvested at 2.5 days post treatment (dpt). Postnuclear supernatant containing organelles was collected from the mock and infected roots used for IP with antibodies against GFP (Groen *et al*., 2014). The extracted proteins from immunoisolated samples were analyzed by LC-MS/MS. In total, 79 entities were found in ARA7-YFP IP profiles, and 46 entities were found in free-GFP IP profiles, to have differential MS2 spectra detection in mock and infected samples (Appendix I). Among them, we selected the entities with a minimum of total 5 MS2 spectra from 4 experiments, and a predicted PM localization (UniProt). Finally, we focused on the proteins enriched in ARA7-IP profiles upon infection and not detected in the free-GFP IP profiles. A leucine-rich repeat receptor-like kinase, MATERNAL EFFECT EMBRYO ARREST 39 (MEE39, At3g46330), fit these criteria (Table 1) and was identified as a potential plant receptor required for plant resistance to Fo.

**Table 1. MS2 spectra detection of MEE39 from MVB/PVC IP analysis upon Fo5176 infection.** Arabidopsis seedlings expressing the MVB/PVC specific marker ARA7-GFP or the negative control free-GFP were exposed to Fo microconidia and grown in hydroponic culture. Mock and infected roots were harvested 2.5 days post treatment (dpt). Immuno-isolation and the following LC-MS/MS analysis were performed as described in the methods. The MS2 spectra detected from four (1-4) experiments of mock (m) and infected (i) samples are shown. The average spectra count representing MEE39 in the ARA-IP profile was significantly higher in the infected than in the mock, while no significant difference was detected between tretaments in the GFP spectra counts.

| **ARA7-YFP IP profile** | | | | | | | | |
|---|---|---|---|---|---|---|---|---|
| | MS2 Spectra Count (Protein Identification Probability) | | | | | | | |
| **Identified Proteins** | ARA7-YFP_m_1 | ARA7-YFP_m_2 | ARA7-YFP_m_3 | ARA7-YFP_m_4 | ARA7-YFP_i_1 | ARA7-YFP_i_2 | ARA7-YFP_i_3 | ARA7-YFP_i_4 |
| **MEE39** | 1 (99%) | 0 (0%) | 1 (78%) | 1 (94%) | 3 (100%) | 2 (100%) | 2 (100%) | 2 (100%) |
| **GFP** | 48 (100%) | 91 (100%) | 31 (100%) | 42 (100%) | 42 (100%) | 30 (100%) | 46 (100%) | 84 (100%) |

| **Free-GFP IP profile** | | | | | | | | |
|---|---|---|---|---|---|---|---|---|
| | MS2 Spectra Count (Protein Identification Probability) | | | | | | | |
| **Identified Proteins** | free-GFP_m_1 | free-GFP_m_2 | free-GFP_m_3 | free-GFP_m_4 | free-GFP_i_1 | free-GFP_i_2 | free-GFP_i_3 | free-GFP_i_4 |
| **MEE39** | Not detected | | | | | Not detected | | |
| **GFP** | 48 (100%) | 83 (100%) | 83 (100%) | 119 (100%) | 86 (100%) | 52 (100%) | 110 (100%) | 75 (100%) |

To test the role of MEE39 in plant defense against Fo5176, we subjected a T-DNA knock-out mutant of MEE39, which is designated as *mee39-1* (Fig. S2), to an *in vitro* plate infection assay using Fo5176 *pSIX1:GFP*. This assay provides the opportunity to observe for the fungal vascular penetration, which is the key step of Fo infection, together with the root growth inhibition (Kesten *et* al., 2019; Huerta *et al*., 2020). At 6 days post treatment (dpt), *mee39-1* mutants exhibited a root growth similar to wild-type plants, which was decreased by 40.2% upon Fo5176 infection (Fig 1a, b). At 7 dpt, more fungal vascular penetrations were observed in the *mee39-1* mutant (3.5 penetration sites / root) than the wild type (2.0 penetration sites / root) (Fig. 1c). To verify the role of MEE39 in root defense against Fo, we transformed *pMEE39:MEE39-GFP* into the *mee39-1* mutant (designated as *MEE39-GFP* hereafter) and tested for *pSIX1:GFP* Fo5176 vascular penetration. This complementation rescued the deficiency in *mee39-1* to wild-type levels (2.1 penetrations / root) (Fig. 1c). These results support the contribution of MEE39 to root defense against Fo5176 vascular penetration. To examine whether MEE39 is required for defense against the wilting caused by Fo, we tested *mee39-1* mutants with an infection assay on soil. At 14 dpt, *mee39-1* mutants displayed more severe wilting symptoms than wild-type plants, which resulted in a higher disease score in *mee39-1* mutants than that in wild-type plants (Fig S3a, b). We also tested if MEE39 has a role in defense against other wilting diseases such as bacterial wilt caused by *Ralstonia solanacearum*. At 18 dpt exposure to this bacteria in soil, *mee39-1* mutants showed more wilting symptoms and a higher disease score compared to wild-type plants (Fig. S3c, d).

Taken together, these data suggest that MEE39 could be also required for defense against bacterial wilt. These results indicate that MEE39 is required in plant defense against vascular pathogens from different Kingdoms.

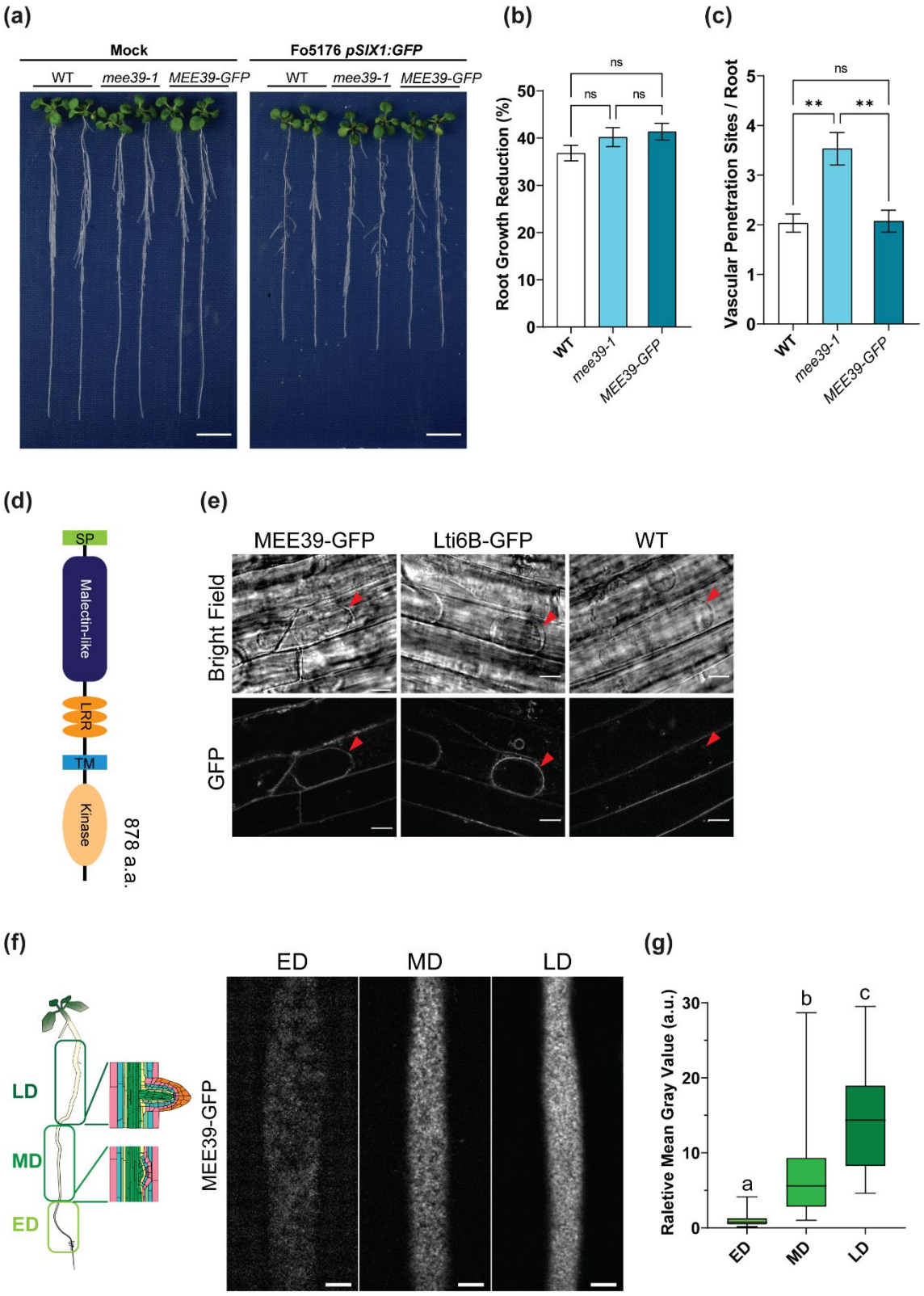

**Figure 1. MEE39 is a PM localized receptor-like protein contributing to root defense against Fo infection.** (a) Representative images of WT, *mee39-1*, and the *MEE39-GFP* seedlings 6 days post treatment (dpt) with Fo5176 *pSIX1:GFP* spores. Scale bars = 1 cm. (b) Quantification root growth reduction caused by Fo5176 *pSIX1:GFP* infection at 6 dpt. $N \geq 55$ roots were obtained from 3 experiments (≥ 15 roots/experiment were used). Values are Av ± SE. The data were analyzed by one-way ANOVA followed by Dunn's multiple comparisons test. ns, not significant. (c) Root vascular penetration of WT, *mee39-1*, and the *MEE39-GFP* at 7 dpt. $N \geq 50$ roots were obtained from 3 experiments (≥ 15 roots/experiment were used). Values are Av ± SE. The data were analyzed by one-way ANOVA followed by Dunn's multiple comparisons test. $^{**}P \leq 0.01$. ns, not significant. (d) Scheme of *in silico* predicted protein structure of MEE39 using UniProt (https://www.uniprot.org/). SP, signal peptide. TM, transmembrane domain. a.a., amino acids. (e) Representative spinning disk confocal images of plasmolysed root epidermal cells expressing MEE39-GFP or Lti6B-GFP. The wild-type roots were included as control for cell wall autofluorescence. Ten-day-old roots were treated with 0.8 M mannitol for 10 min and the middle differentiated zone (see (f)) was imaged. Two experiments were performed with similar results. Red arrowheads indicate plasma membrane that is detached from the cell wall. Scale bar = 10 μm. (f) Representative images of root epidermal cells expressing MEE39-GFP. Left panel illustrates root zones defined in this study. ED, early differentiation zone. MD, middle differentiation zone. LD, late differentiation zone. Right panel shows representative spinning disk confocal images of MEE39-GFP at the indicated root differentiated zones. Scale bars = 5 μm. (g) Quantification of the mean gray value (arbitrary units, a.u.) of GFP signal intensity of MEE39-GFP as depicted in (f). The mean gray values were normalized to the average in the ED. Box plots: centerlines show the medians; box limits indicate the 25th and 75th percentiles; whiskers extend to the minimum and maximum. $N \geq 21$ cells were obtained from 3 experiments (2-4 cells/root and ≥ 3 roots/experiments were imaged). Data were analyzed with one-way ANOVA followed by Dunn's multiple comparisons test. Alphabet letters indicate significant differences by $P < 0.05$.

Based on *in silico* analysis, MEE39 is a member of the LRR-RLK I family characterized by an extracellular malectin-like domain and LRR repeats, followed by a transmembrane domain and a cytosolic kinase domain, and its homologs are only found in Brassicales (Fig. 1d, Table S1). To confirm the predicted subcellular localization of MEE39, we performed a plasmolysis experiment using seedlings expressing *MEE39-GFP*. We always observed MEE39-GFP anchored to the plasmolyzed PM, clearly detached from the autofluorescent cell wall, as the PM marker line LOW TEMPERATURE INDUCED 6B-GFP (Lti6B-GFP; Cutler *et al.,* 2000; Fig. 1e). Furthermore, we examined the MEE39-GFP PM localization at the subcellular level of root epidermal cells using spinning disc confocal microscopy. We examined the protein localization in the early differentiated zone (ED), the middle differentiated zone (MD), and the late differentiated zone (LD), which are marked by the emergence of root hairs, the presence of the first lateral root primordium initiation, and the first emerged lateral root, respectively (Fig. 1f, left panel). The MEE39-GFP signal was only detectable after the elongation zone, increasing with the differentiation level of the cells from ED to LD, but weakly in the ED (Fig. 1f, 1g). These results indicated that a higher intensity of MEE39-GFP was detected in more mature root tissues at the epidermal layer, which suggests MEE39 protein accumulation gradually increases along the root axis.

*MEE39 proteins and transcript levels respond to Fo5176 infection*

To characterize MEE39 in root-Fo5176 interaction, we investigated changes of MEE39-GFP protein changes in root MD epidermal cells, where MEE39-GFP was strongly detected. We exposed MEE39-GFP expressing seedlings to Fo5176 pre-germinated spores for 1 day. The PM-resident SNARE protein marker NPSN12-YFP (Geldner *et al*., 2009) was included as control. In Fo5176 treated cells, the intensity of MEE39-GFP was significantly decreased to around 30% of that in mock treated ones, while NPSN12-YFP signals were not affected by the fungus (Fig. 2a, 2b). These data indicated that MEE39 protein accumulation at the PM of root epidermal cells decreased in response to Fo5176. To confirm these results, we studied the changes in the MEE39-GFP protein amount in the lower part of the roots (MD and below; Fig 2c left panel) when exposed to Fo5176. Indeed, Western blotting revealed decreased MEE39-GFP but no alteration of the SYP21 (MVB/PVC membrane localized SNARE protein; Tse *et al*., 2004) levels upon Fo5176 pre-germinated spores treatment for 1 day (Fig 2c, 2d). These results confirmed that the reduced MEE39 protein levels in response to Fo5176 was not a consequence of a general protein decrease, as NPSN12-YFP intensity at the PM and SYP21 protein levels remained unaltered.

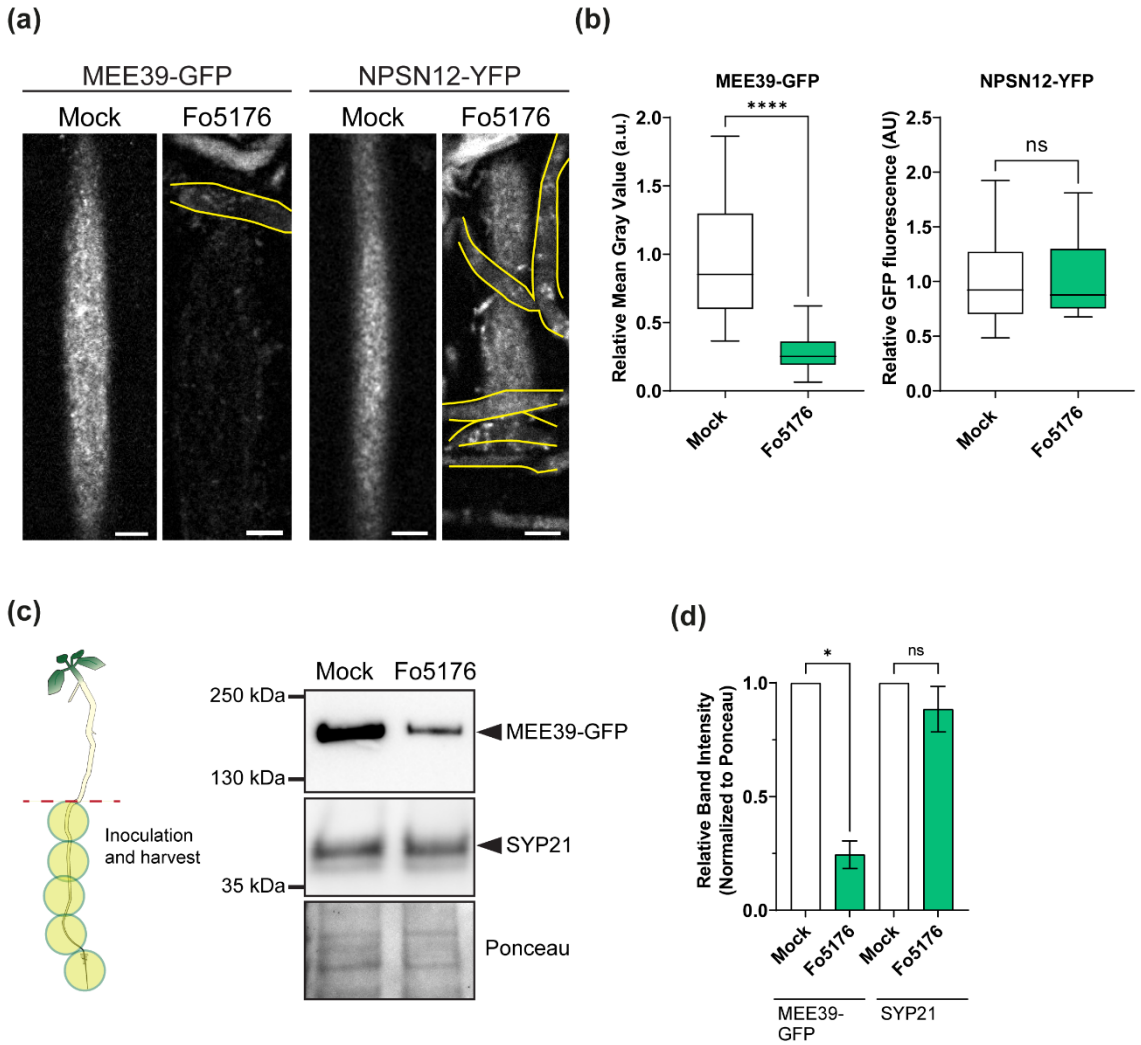


**Figure 2. MEE39-GFP protein accumulation is decreased by Fo5176 treatment.** (a) Representative spinning disk confocal images of 8-day-old root epidermal cells in the MD expressing MEE39-GFP or NPSN12-YFP after 1-day exposure of pre-germinated Fo5176 spores. The yellow lines indicated the Fo5176 hyphae. MEE39-GFP was hardly detected in the infected epidermal cells in the MD. Scale bars = 5 μm. (b) Quantification of GFP intensity by measuring mean gray value from the images as shown in (a). Areas-of-interest was selected manually to avoid the hyphae. $N \geq 17$ cells were obtained from 3 experiments (2-4 cells/root and ≥ 3 roots/experiments were imaged). Box plots: centerlines show the medians; box limits indicate the 25th and 75th percentiles; whiskers extend to the minimum and maximum. For each marker, the intensity of fungal-exposed sample was normalized to that of mock. Data were analyzed by *t*-test. ****$P \leq 0.0001$. ns, not significant. (c) Representative image of Western blot detecting MEE39-GFP and SYP21. Eight-day-old MEE39-GFP roots were pre-germinated Fo5176 spores for 1 day. The left panel illustrates the root tissue that was treated and harvested: the green circles indicate where the drops containing the fungus were placed, and the tissue below the red dashed line was harvested. The blot was stained with Ponceau S to show the total protein amounts. (d) Quantification of the band intensity from Western blot ash shown in (c). For each protein, the intensity of fungal-exposed sample was normalized to that of mock. Two experiments were performed and Av ± SE is shown in the graph. Data were analyzed by *t*-test. *$P < 0.05$. ns, not significant.

To test whether the reduction of MEE39 protein level by Fo5176 treatment was regulated transcriptionally, we generated the *pMEE39:mCherry-N7* marker line. The N7 peptide targets the mCherry fluorescent protein to the nucleus (Cutler *et al.,* 2000), serving as a fluorescent reporter of *MEE39* promoter activity. Under mock conditions, the mCherry signal was very weak in the transition and elongation zones (TZ-EZ; 3.03 ± 0.15 a.u.) and in the ED (6.82 ± 0.52 a.u.), and was greatly enhanced in the MD (160.05 ± 5.00 a.u.; Fig. 3a, b). After the roots were exposed to Fo5176 pre-germinated spores for 1 day, the mCherry signal increased in all 3 tested regions: 7.60 ± 0.97 a.u., 30.79 ± 2.21 a.u., and 214.58 ± 2.55 a.u. in TZ-EZ, ED, and MD zones, respectively (Fig 3a, b). Such enhancement of mCherry signals was more dramatic after the roots were treated for 3 days while the mock roots exhibited similar mCherry signal patterns at both time points. At 3 dpt, the infected roots exhibited clear developmental changes in the region close to the meristem that may correspond to the TZ-EZ in mock roots. This area with bulged cells and abundant root hairs was designated as the stress zone (SZ) and showed a very high mCherry fluorescence compared to the mock and 1 day-exposed TZ-EZ zone (127.20 ± 6.52 a.u. in SD; 7.60 ± 0.97 a.u. in TZ-EZ 1 day; Fig. 3, S4). The ED also exhibited higher mCherry signal after 3 days of fungal exposure than that observed at 1 day (136.57 ± 6.56 a.u. at 3 dpt and 30.79 ± 2.21 a.u. at 1 dpt; Fig. 3, S4), but less dramatic than the changes observed in the SZ. The MD response to the fungus was not altered by a longer exposure (190.89 ± 3.65 a.u. at 3 dpt and 214.58 ± 2.55 a.u. at 1 dpt; Fig. 3, S4). These data indicated that *MEE39* promoter activity is activated by Fo5176. The *MEE39* mRNA accumulation in mock and Fo5176-plate infected roots was then examined by qRT-PCR at different times after fungal exposure. The results showed that *MEE39* transcript levels gradually increased while the fungal infection progressed. At 7 dpt, the relative expression level of *MEE39* in the infected roots was 2-fold higher than that in mock treated roots (Fig. 3c). Taken together, our data revealed that the transcription of *MEE39* was activated by Fo5176 infection, while the MEE39 protein accumulation was decreased.

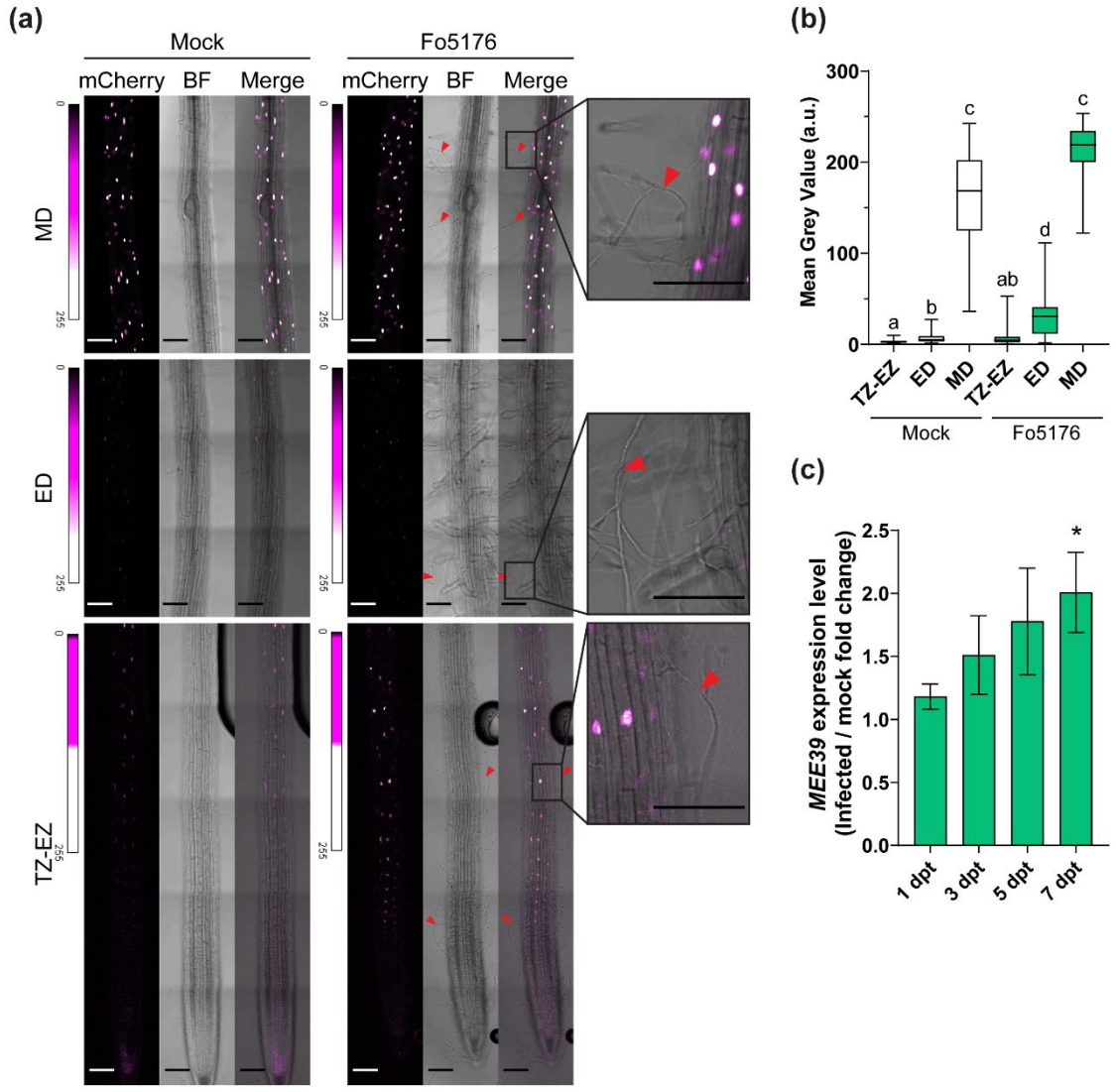


**Figure 3. *MEE39* transcription is activated by Fo5176 treatment.** (a) Representative confocal images of 8-day-old root epidermal cells expressing *pMEE39:mCherry-N7* after 1-day exposure of pre-germinated Fo5176 spores. mCherry signal intensities are displayed as the relative heatmaps. BF, brightfield. TZ-EZ, transition zone to elongation zone. ED, early differentiation zone. MD, middle differentiation zone. Red arrowheads indicate fungal hyphae. Scale bars = 100 μm. (b) Quantification of the mCherry signal intensity at different root developmental zones after Fo5176 hyphae contact as depicted in (a). $N \geq 95$ cells were obtained from 3 experiments (≥ 6 cells/root and 3 roots/experiment were imaged). Box plots: centerlines show the medians; box limits indicate the 25th and 75th percentiles; whiskers extend to the minimum and maximum. Data were analyzed by one-way ANOVA followed by Dunn's multiple comparisons test. Alphabet letters indicate significant differences with $P < 0.05$. (c) *MEE39* expression relative to *AtGAPDH* in 8-day-old WT roots at different dpt of exposure to Fo5176 *pSIX1:GFP* spores containing plates. The relative *MEE39* expression in fungal-treated sample is normalized to that of mock-treated. Four experiments were performed (≥ 20 roots/experiment were used). Values are Av ± SE. Data were analyzed by *t*-test comparing to the fold change at 1 dpt. $*P < 0.05$.

*Immunity marker gene expressions are activated in mee39-1 mutant by Fo5176 infection*

To test the role of MEE39 as a receptor, we tested whether defense signaling was affected in *mee39*-1 by assessing downstream gene expression using qRT-PCR. We selected immunity marker genes that were previously known to respond to Fo5176 infection (Lyons *et al*., 2015; Masachis *et al*., 2016; Kesten *et al*., 2019). These genes include stress responsive transcription factors, *WRKY45* and *WRKY53* (Masachis *et al*., 2016; de Azevedo Souza *et al*., 2017), ISX-inducible genes, *FRK1* and *CYP81F2* (Van der Does *et al*., 2017), and peroxidase encoding gene, *PRX33* (Lyons *et al*., 2016). The transcript levels of all these genes were up-regulated in the wild type by the Fo5176 infection (Fig. S5a-d). At 3 dpt, 4 of the genes tested in *mee39-1* did not reach the activation level as in the wild type (Fig. S5b), and this difference was not complemented in the *MEE39-GFP* transformant, except for the expression of *CYP81F2*. These genes were later analyzed at 5.5 dpt. In wild-type plants, these genes continued to be up-regulated (Fig. S5c, d). Compared to those in the wild-type and *MEE39-GFP* roots, these downstream genes expression in *mee39-1* roots was more enhanced (Fig. S5d). The fungal colonization was also assessed by normalizing the transcript level of Fo5176 *β-tublin* to the transcript level of plant *GAPDH*, and a higher accumulation of Fo5176 *β-tublin* mRNA was found in *mee39-1* than in both the wild type and *MEE39-GFP* at 5.5 dpt. This result is consistent with the higher vascular penetrations found in *mee39-1* roots at 7 dpt (Fig. 1c). Taken together, the upregulation of these tested genes seems to be delayed in *mee39-1* compared to the wild type.

*MEE39 could be required for plant response to cellulose synthesis inhibition*

MEE39 contains an extracellular malectin-like domain, which is also present in receptor kinases of the CrRLK1L family participating in cell wall integrity sensing and signaling (Hématy *et al*., 2007; Van der Does *et al*., 2017). Our previous data revealed that cellulose synthesis inhibition is an essential cell wall remodeling process in response to Fo5176 (Kesten *et al.,* 2019; Menna *et al*., 2021). Therefore, considering that the malectin-like domain of MEE39 might imply its role in sensing cell wall integrity during Fo5176 infection, we investigated its potential role in cellulose integrity sensing by evaluating the *mee39-1* response to the cellulose chemical inhibitor isoxaben (ISX; Desprez *et al*., 2002). The ISX treatment induced root swelling and a 52.1% of root growth reduction in the wild type (fig. 4a, b). The root growth was as well reduced in *mee39-1* mutant by the ISX treatment, but the reduction (48.8%) was significantly lower than that of the wild type (Fig. 4b). In the *MEE39-GFP* complemented line, the root growth reduction (51.3%) was rescued to the wild-type

level. The results support the claim that MEE39 is required for plant response to cellulose synthesis inhibition induced by ISX.

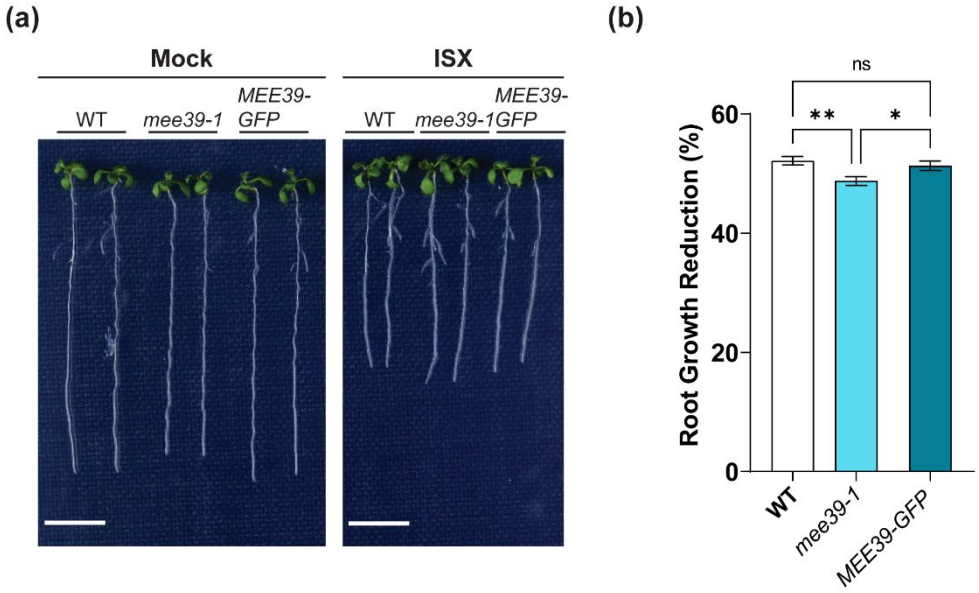


**Figure 4. *mee39-1* mutant is less sensitive to isoxaben than wild-type plants.** (a) Representative image of 5-day-old WT, *mee39-1*, and *MEE39-GFP* plants treated with mock or 2 nM isoxaben (ISX) at 5 dpt. Scale bars = 1 cm. (b) Quantification of normalized root growth reduction in seedlings as depicted in (a). $N \geq 65$ roots were obtained from 4 experiments (≥ 15 roots/experiments were used). Values are Av ± SE. Data were analyzed by one-way ANOVA followed by Tukey's multiple comparisons test. $*P < 0.05$, $**P \leq 0.01$, ns: not significant.

We then analyzed the MEE39-GFP protein abundance at the PM in ED and MD epidermal root cells after 1 day of ISX treatment, following the same method used in response to Fo5176 pre-germinated spores (Fig. 2). The MEE39-GFP intensity in ED cells was 3-fold higher in ISX-treated than in mock-treated cells, while the MD cells did not respond significantly to ISX (Fig. 5a, b). Consistently with the observed enhancement of MEE39-GFP signals under the microscope, a higher level of total MEE39-GFP protein amount was detected in the Western blot upon the ISX treatment (Fig. 5c, d). These data indicate that MEE39 protein levels increase in response to chemically induced cellulose synthesis inhibition.

To examine whether the enhancement of MEE39-GFP protein by ISX was regulated on *MEE39* transcription, we tested the *pMEE39:mCherry-N7* marker upon the ISX treatment. After 1 day of ISX treatment, the mCherry signal was greatly enhanced in the ISX-induced SZ and ED (63.12 ± 1.35 and 125.54 ± 3.79 a.u.) compared to the mock TZ-EZ and ED (3.35 ± 0.11 and 11.7 ± 0.42 a.u.; Fig. 6a, b). The MD cells also exhibited higher mCherry signal upon ISX treatment (172.38 ± 3.24 a.u.) than that in the mock (115.06 ± 3.14 a.u.), but this change was less dramatic than that observed in the younger tissues (Fig. 6a, b). These

observations revealed that *MEE39* transcription is activated by ISX, which correlates to the enhanced MEE39 protein accumulation at the PM in response to ISX.

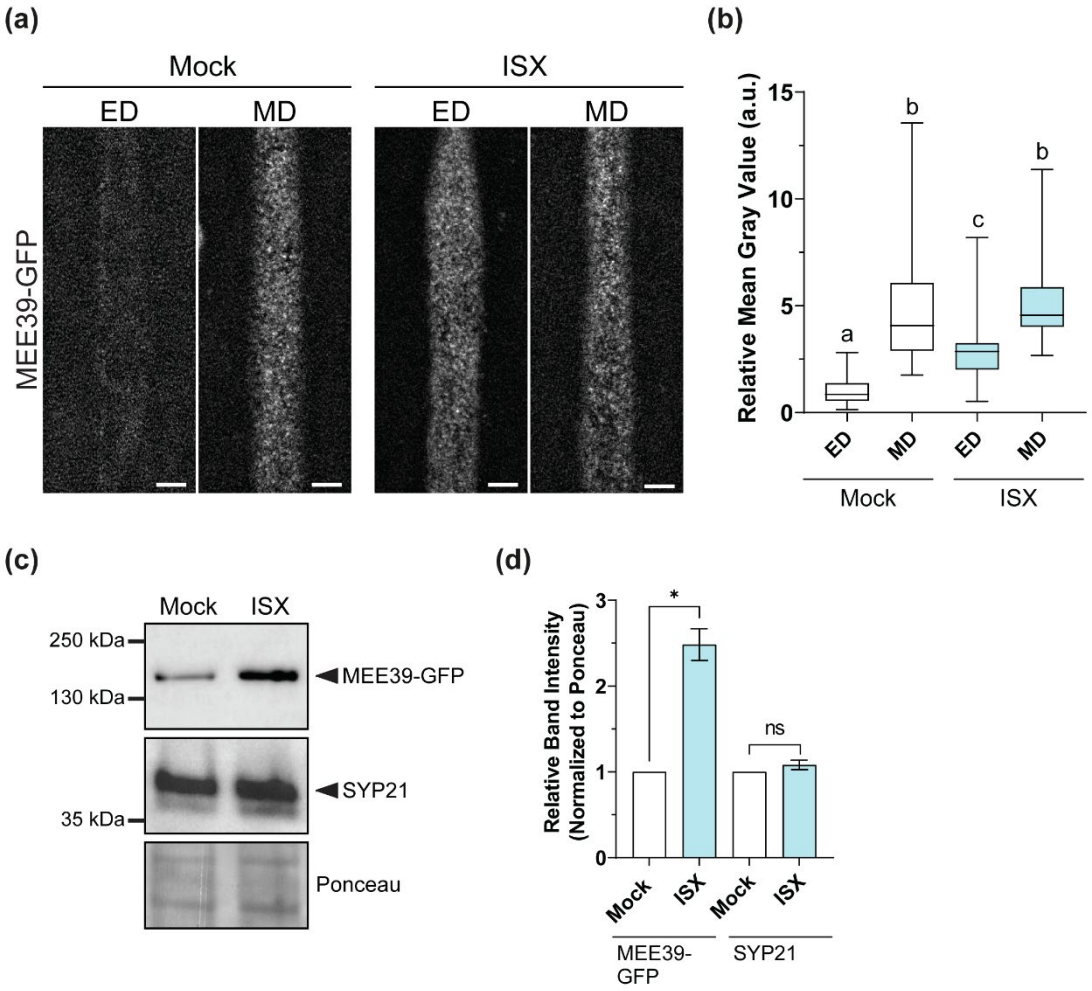


**Figure 5. MEE39-GFP protein accumulation is enhanced by isoxaben treatment.** (a) Representative spinning disk confocal images of 8-day-old root epidermal cells in the ED expressing MEE39-GFP in response to 300 nM isoxaben (ISX) treatment for 1 day. Scale bars = 5 μm. (b) Quantification the GFP intensities intensity by measuring mean gray value from the images as shown in (a). $N \geq 41$ cells were obtained from 3 experiments (3-5 cells/root and ≥ 3 roots/experiments were imaged). Box plots: centerlines show the medians; box limits indicate the 25th and 75th percentiles; whiskers extend to the minimum and maximum. The intensity values were normalized to that of mock-treated ED. Data were analyzed by one-way ANOVA followed by Dunn's multiple comparisons test. Alphabet letters indicate significant differences with $P < 0.05$. (c) Representative image of Western blot detecting MEE39-GFP and SYP21. Eight-day-old MEE39-GFP roots were treated with 300 nM ISX for 1 day. The blot was stained with Ponceau S to show the total protein amounts. (d) Quantification of the band intensity from Western blot ash shown in (c). For each protein, the intensity of ISX-treated sample was normalized to that of mock. Two experiments were performed and Av ± SE is shown in the graph. Data were analyzed by *t*-test. $*P < 0.05$. ns, not significant.

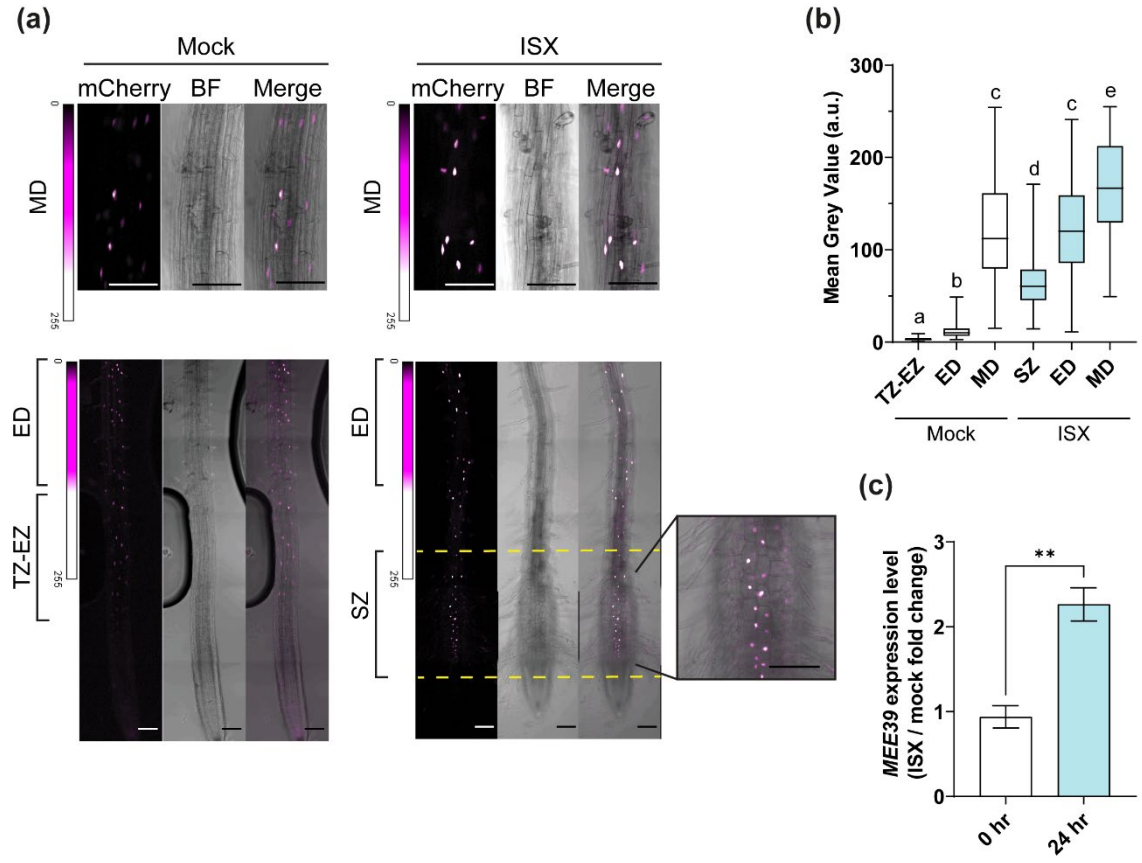


**Figure 6. *MEE39* transcription is activated by isoxaben treatment.** (a) Representative confocal 8-day-old root epidermal cells expressing *pMEE39:mCherry-N7* after 1-day treatment of 300 nM ISX. mCherry signal intensities are displayed as the relative heatmaps. BF, birghtfield. TZ-EZ, transition zone to elongation zone. ED, early differentiation zone. MD, middle differentiation zone. SZ, stress zone. Scale bars = 100 μm. (b) Quantification of the mCherry signal intensity at the different root developmental zones as depicted in (a). $N \geq 208$ cells were obtained from 3 experiments (≥ 6 cells/root and 6 roots/experiment were imaged). Box plots: centerlines show the medians; box limits indicate the 25th and 75th percentiles; whiskers extend to the minimum and maximum. Data were analyzed by one-way ANOVA followed by Dunn's multiple comparisons test. Alphabet letters indicate significant differences with $P < 0.05$. (c) *MEE39* expression relative to *GAPDH* in 8-day-old WT roots after 1-day treatment of 300 nM ISX. The relative *MEE39* expression in ISX-treated sample is normalized to that of mock-treated. Four experiments were performed (≥ 20 roots/experiment were used). Values are Av ± SE. Data were analyzed by *t*-test comparing to the fold change at 1 dpt. $*P < 0.05$.

*MEE39 could function with MIK2 in plant defense against Fo5176 infection, but it is unclear whether the two participate in the same cellulose integrity-sensing pathway*

To deepen the understanding of molecular mechanism of MEE39 function, we identified MEE39 interacting proteins during root-Fo5176 interaction utilizing a pull-down assay with MEE39-GFP roots and including the Lti6B-GFP PM marker as the background-binding control. As a result, the LRR-RLK protein, MIK2, was found to be enriched in MEE39-GFP IP, but not in Lti6B-GFP IP, upon Fo5176 infection (Appendix II, Table 2). MIK2 was previouly reported to participate in plant response to ISX and to be required in plant defense

against Fo5176 (Van der Does *et al*., 2017; Coleman *et al*., 2021). These studies are in line with our data obtained from the analysis of *mee39-1* (Fig. 1, 4), implying a potential functional relation between MIK2 and MEE39 in plant response to Fo5176 and cellulose synthesis inhibition.

**Table 2. Detection of MIK2 from MEE39-GFP pull-down assay upon Fo5176 infection.**
Arabidopsis seedlings expressing MEE39-GFP and the plasma membrane specific marker Lti6B-GFP (negative) were exposed to Fo microconidia and grown in hydroponic culture. Mock and infected roots were harvested 3 days post treatment (dpt). Immuno-isolation and the following LC-MS/MS analysis were performed as described in the methods. The MS1 spectra from 3 experiments were analyzed with label-free quantification to compare mock and infected samples, and the one-way ANOVA p-values are given. Significant differences were indicated by alphabet letters.

| | | LFQ intensity (a.u., Av±SD) | | | | | | |
|---|---|---|---|---|---|---|---|---|
| **Name** | AGI | Lti6B_ Mock | Lti6B_ Infected | MEE39_ Mock | MEE39_ Infected | ANOVA p-value | MS/MS count | Unique peptides |
| **MEE39** | AT3G46330 | 0 ± 0, a | 0 ± 0, a | 31.17 ± 0.42, b | 31.21 ± 1.23, b | 4.32E-12 | 642 | 39 |
| **MIK2** | AT4G08850 | 0 ± 0, a | 0 ± 0, a | 6.90 ± 11.9, b | 24.15 ± 3.09, c | 0.0041 | 42 | 23 |

To test this hypothesis, the *mee39-1 mik2-1* double mutant was generated and subjected to plate Fo5176 infection assay and ISX treatment. The *mik2-1* roots were more susceptible to Fo5176 infection as they showed increased growth reduction and higher number of fungal vascular penetrations than wild-type plants (Fig. 7a-c). Our data suggest that the role of MIK2 in plant defense to Fo5176 might be regulated in roots and explain the higher wilting and dead symptoms observed in aerial parts of *mik2-1* during Fo5176 soil infections (Van der Does *et al*., 2017). The *mee39-1 mik2-1* double mutant showed the same susceptibility to Fo5176 as *mik2-1* both at the level of root growth inhibition and vascular penetration, which was higher than the *mee39-1* susceptibility (Fig 7a-c). These data suggest that MEE39 and MIK2 function in the same pathway in root defense against Fo5176.

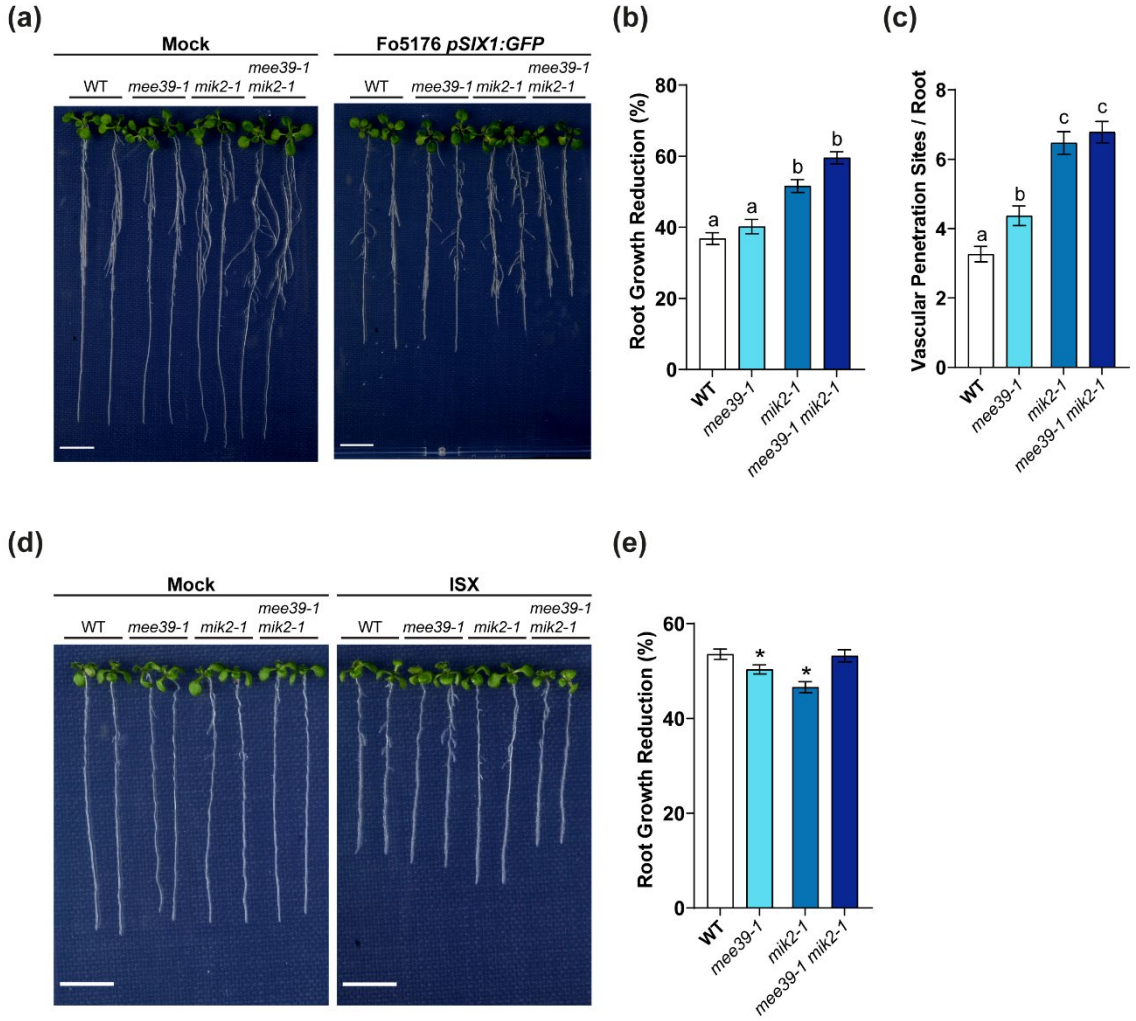


**Figure 7. *MIK2* is involved in the same pathway with *MEE39* in plant defense against Fo, but whether they function in the same sensing pathway to ISX remains unclear.** (a) Representative images of WT, *mee39-1*, *mik2-1*, and *mee39-1 mik2-1* mutants 6 days post treatment (dpt) with Fo5176 *pSIX1:GFP* spores. Scale bars = 1 cm. (b) Quantification root growth reduction caused by Fo5176 *pSIX1:GFP* infection at 6 dpt. $N \geq 55$ roots were obtained from 3 experiments (≥ 15 roots/experiment were used). Values are Av ± SE. Data were analyzed by one-way ANOVA followed by Dunn's multiple comparisons test. ns, not significant. (c) Root vascular penetration of WT, *mee39-1*, *mik2-1*, and *mee39-1 mik2-1* mutants at 7 dpt. $N \geq 73$ roots were obtained from 4 experiments (≥ 15 roots/experiment were used). Values are Av ± SE. Data were analyzed by one-way ANOVA followed by Dunn's multiple comparisons test. Alphabet letters indicate significant differences by $P < 0.05$. (d) Representative image of 5-day-old WT, *mee39-1*, *mik2-1*, and *mee39-1 mik2-1* mutants treated with mock or 2 nM isoxaben at 5 dpt. Scale bars = 1 cm. (e) Quantification of normalized root growth reduction in seedlings as depicted in (d). $N \geq 45$ roots were obtained from 3 experiments (≥ 15 roots/experiments were used). Values are Av ± SE. Data were analyzed by *t*-test to compare with the wild type. $*P < 0.05$.

MIK2 has been recently identified as the receptor for the SERINE RICH ENDOGENOUS PEPTIDE12 (SCOOP12) phytocytokine and suggested to recognize Fo-derived SCOOP-like peptides to induce immunity against this fungi (Coleman *et al*., 2021; Rhodes *et al*., 2021). Thus, we tested whether MEE39 is involved in plant response to SCOOP12 by assessing the

root growth inhibition caused by the peptide. Unlike *mik2-1* root growth remaining unaltered by SCOOP12 treatment, *mee39-1* root growth was reduced to the wild-type level by the treatment (Fig. S6). Therefore, our data suggest that MEE39 is not involved in MIK2-dependent response to SCOOP12.

As MIK2, MEE39 has a role in sensing ISX. Therefore, we clarified the genetic interaction of MEE39 and MIK2 in sensing cellulose synthesis inhibition induced by ISX. Compared to *mee39-1*, *mik2-1* was more resistant to ISX treatment (Fig. 7d, e). Unexpectedly, *mee39-1 mik2-1* restored the root response to ISX to the wild-type level (Fig. 7e). This genetic analysis suggests that the plant response to ISX could be complemented by another signaling pathway independent of MEE39 and MIK2 when both genes are impaired. Taken together, MEE39 and MIK2 participate in the plant defense mechanism against Fo5176 that is independent of sensing SCOOP12 and ISX.

**Discussion**

*MEE39 contributes to plant defense against wilting diseases*

The mechanisms of plant recognition of and defense against Fo are largely unexplored. In this study, we took advantage of MVB / PVC immunoisolation to identify a new PM protein involved in this process, MEE39 (Table 1). MVB / PVC is a canonical center to collect proteins before transporting them to the vacuole for degradation (Fig S1, Robinson *et al.,* 2008; Ben Khaled *et al*., 2015). Therefore, the enrichment of MEE39 in MVB / PVC IP during Fo infection may indicate an enhancement of MEE39 vacuolar degradation upon the signal perception, which is a known mechanism for regulating PM receptors activating plant defense (Ben Khaled *et al*., 2015). We then tested a T-DNA knock-out mutant, *mee39-1*, to characterize the function of MEE39. *mee39-1* displayed a root growth similar to the wild type with or without Fo infection (Fig. 1a, b). The developmental phenotype of *mee39-1* revealed that the function of MEE39 may be independent of its originally suggested role in embryo development, which gave the name of MEE39 by the arrested endosperm phenotype in a *Ds* transposon insertion mutant (Pagnussat *et al*., 2004). In this original MEE39 study, the *mee39* mutant was not examined for additional mutation nor complemented by transforming *MEE39*, therefore, it is possible that the embryonic deficiency in this mutant is a pleiotropic effect. To clarify such effect in *mee39-1*, we used the *MEE39-GFP* complementation line in our study. In-plate and in-soil Fo infection assays using *mee39-1* indicated that MEE39 contributes to plant resistance to Fo (Fig. 1c, S3a, b). Furthermore, the soil assays revealed that MEE39 contributes to plant defense against wilting diseases caused not only by Fo, but also by

another bacteria vascular pathogen *Ralstonia solanacearum* (Fig. S3c, d). Both Fo and *Ralstonia solanacearum* reach the root vasculature and colonize it without extensive proliferation in root cell layers outside the vasculature (Digonnet *et al*., 2012; Menna *et al*., 2021). The enhanced wilting symptoms observed in *mee39-1* indicated that MEE39 facilitates plant defense to reduce/slow down pathogen entrance and/or proliferation in the vasculature, and the later water transport blockage. These data together with the results obtained from the in-plate Fo infection assay monitoring vascular penetration (Fig. 1c), revealed that MEE39 likely functions already before the pathogens enter the vasculature.

Based on *in silico* analysis, MEE39 belongs to the LRR-LRK I family that might act as sensors of apoplastic signals through their malectin-like domain and/or LRR domains (Fig. 1d; Rui & Dinneny, 2020). Other members of the same family, such as Impaired Oomycete Susceptibility 1 (IOS1) and STRESS INDUCED FACTOR 2 (SIF2), have been shown to be receptor-like kinases located at the PM and mediating plant signaling (Hok et al., 2011; Hok et al., 2014; Yuan et al., 2018). In this study, MEE39 is a newly characterized LRR-LRK I member localized at the PM in root epidermal cells (Fig. 1e, f), suggesting that it may activate signaling in the outermost layer of the root. Therefore, the examination of MEE39 in root epidermal cells became the focus of this study. MEE39-GFP protein was not evenly distributed along the root, which was only detected in the differentiated zone (Fig. 1f) despite that *MEE39* promoter activity was observed using *pMEE39:mCherry-N7* marker in the transition and elongation zones (Fig 3a), and its signal became stronger along the root axis in the MD and LD (Fig. 1f, g). These expression patterns indicated different capacities of MEE39 signaling in different tissues, which is greater in more mature root tissues.

We found that these gradient-like patterns of MEE39 expression could be further regulated by Fo5176, resulting in severely reduced MEE39-GFP protein levels in the MD (Fig. 2). The data revealed a lower MEE39-GFP intensity at the Fo5176-treated PM (Fig. 2b). Consistently, total MEE39-GFP protein amount was decreased in the examined tissue (Fig. 2c, d). This protein reduction seems to be MEE39-specific, as other membrane proteins, NPSN12 and SYP21, were not affected by the infection (Fig. 2b, d). However, *MEE39* transcription was activated by Fo5176. The *MEE39* promoter activity in the TZ-EZ, ED, and MD, was enhanced by the infection, and accordingly, the *MEE39* transcript level was elevated (Fig. 3, S4). Moreover, the activation of *MEE39* promoter activity and transcript level became stronger as the infection progressed (Fig. 3c, S4). These data indicated that *MEE39* transcription was boosted while its protein level was decreased by the Fo5176, which suggests that MEE39-dependent signaling needs to be attenuated at the PM.

As a receptor-like kinase, MEE39 might participate in regulating downstream gene expression required for plant immunity. To test this hypothesis, we analyzed the immunity marker gene expressions reported to respond to Fo infection (Lyons *et al*., 2015; Masachis *et al*., 2016; Kesten *et al*., 2019; Menna *et al*., 2021) in *mee39-1*. Among these selected genes, *WRKY* transcription factors are regulatory hubs involved in plant response to various stresses, such as light, cold, salt, and oxidative stresses (Zentgraf & Doll, 2019). *FRK1* and *CYP81F2* are upregulated by bacterial infection besides fungal infection (He *et al*., 2006), and furthermore, they were shown to be activated by pharmacological cellulose synthesis inhibition (Van der Does *et al*., 2017). At 3 dpt of in-plate Fo infection assay, the activation levels of *WRKYs* and *FRK1* were decreased in *mee39-1*, but these levels were not complemented in the *MEE39-GFP* transformant (Fig. S5b), which suggest that the reduced activation levels could be independent on MEE39 function. The data suggest that *CYP81F2* is the only exception that might be regulated by MEE39 (Fig. S5b). At 5.5 dpt, the activation levels of all the tested genes including *CYP81F2* were more enhanced in *mee39-1* compared to the wild type, which reveals that the signaling activating these genes can still be functional in *mee39-1*, but it is delayed (Fig. S5b, d). These data also indicate that MEE39-GFP seems to only complement the regulation on these tested gene expression at a later time point, which is probably affected by pleiotropic effect in the *mee39-1* mutant (Fig. S5b, d). We also examined the fungal colonization in these samples by normalizing the transcript level of Fo5176 *β-tublin* to that of *AtGAPDH*. By comparing the tested plant lines, the results suggest a correlation between the activation level of immunity marker genes and the amount of fungus detected (Fig. S5b, d, e, f), although in general, a lower level of Fo5176 *β-tublin* expression was detected at 5.5 dpt than that at 3 dpt (Fig. S5e, f), which is likely due to the non-synchronized fungal infection in different experiments. Taken together, these results indicate that MEE39 is not needed for upregulating these immunity marker genes in response to Fo, and the delayed activation of these gene expressions reflects the reduced resistance to Fo in *mee39-1*.

LRR-RLKs at the PM have been suggested to interact with other receptors to induce the signaling (Smakowska-Luzan *et al*., 2018). Likewise, we found a large LRR-RLK, MIK2, being a potential interactor of MEE39 in response to Fo infection (Table 2). Generally, small LRR-RLKs like MEE39 were hypothesized to act as co-receptors of the large LRR-RLKs, which do not bind to ligands directly, but are needed for the full activation of the signaling (Smakowska-Luzan *et al*., 2018). The MIK2-MEE39 receptor pair shares a similar structure with a recently described LRR-RLK pair, CANAR-CAMEL, functioning in auxin transport

(Hajný *et al*., 2020). Here we investigated the MIK2-MEE39 functioning in plant defense. MIK2 has been reported to contribute to plant defense against Fo5176 (Van der Does *et al*., 2017). In this study, the plate infection assay further suggested that MIK2 is involved in root response preventing Fo5176 entrance to the vasculature (Fig. 7c). The genetic analyses using *mee39-1 mik2-1* suggest that MEE39 and MIK2 function in the same pathway in plant defense against Fo independently of the SCOOP12 induced signaling (Fig. 7c, S6). Therefore, we identified a new plant defense mechanism through MEE39 and MIK2 against Fo infection that remains to be clarified in the future.

*MEE39 could be involved in sensing cellulose integrity*

MEE39 possesses an extracellular malectin-like domain, which shares similarity with the extracellular domains of plant cell wall integrity sensors of the CrRLK1L family (Franck *et al*., 2018) like THE1. Mutants deficient in THE1 were less sensitive to ISX-induced cellulose synthesis inhibition and more susceptible to Fo infection (Van der Does *et al*., 2017), which is reminiscent of the role of MEE39 in plant defense. In addition, MIK2 was shown to be involved in sensing pharmacologically induced cellulose synthesis inhibition, which was partially dependent on THE1 (Van der Does *et al*., 2017). Cellulose synthesis inhibition results in bulged cells, which are observed in cellulose deficient mutants and ISX-treated roots (Singh *et al*., 2008; Chaudhary *et al*., 2020). Interestingly, our previous study suggested that Fo also induces cellulose synthesis inhibition (Kesten *et al*., 2019; Menna *et al*., 2021), and consistently, we observed bulged cells characteristic of cellulose deficiency in infected roots (Fig. S4). Inspired by these studies on THE1 and MIK2, and the bulged cell phenotype induced by Fo5176, we asked whether MEE39 is involved in sensing cell wall integrity when cellulose synthesis is inhibited by ISX. Our results suggested that MEE39 is needed for plant response to ISX (Fig. 4). Moreover, *MEE39* expression was enhanced by ISX treatment (Fig. 6). Different from the observation with Fo5176 infection, ISX enhanced MEE39 protein accumulation in the ED and did not affect MEE39 in the MD (Fig. 5a, b). These data revealed that MEE39-dependent signaling is attenuated upon Fo infection, but amplified in response to ISX, which probably correlates to its role in different tissues in the ED and MD.

The roles of MIK2 and MEE39 upon ISX were investigated by the genetic analysis. Agreeing with the previous study (Van der Does *et al*., 2017), *mik2-1* displayed reduced sensitivity to ISX (Fig. 7e). However, this reduction was rescued by the *mee39-1 mik2-1* double mutations, which does not clarify whether MEE39 and MIK2 function in the same pathway sensing cell wall integrity. We deduce that another signaling pathway, for instance, the THE1-dependent

pathway, takes over the signaling upon ISX treatment when both MEE39 and MIK2 are deficient. Because THE1 was shown to participate in MIK2-dependent signaling sensing ISX-induced cellulose synthesis inhibition (Van der Does *et al*., 2017), it is possible that a crosstalk between MEE39-dependent pathway and THE1-dependent pathway through MIK2 switches on the THE1-dependent signaling when both MEE39 and MIK2 are impaired.
In conclusion, we present MEE39 as a potential cell wall integrity sensor that also functions in plant defense against Fo, and a MEE39-MIK2 receptor complex is likely formed to activate this uncharacterized defense mechanism. A coordination between cell wall integrity sensing and plant defense may thus be achieved by the dual functions of MEE39.

**Materials and Methods**

*Plant material and growth conditions*

*Arabidopsis thanliana* wild type (Col-0), and previously described mutants and marker lines, *mik2-1* (SALK_061769) (Van der Does *et al*., 2017), *pUBQ10:ARA7-YFP*, *pUBQ10:NPSN12-YFP* (Geldner *et al*., 2009), *p35S:free-GFP* (Gadeyne *et al*., 2014), and *p35S:Lti6B-GFP* (Cutler *et al.,* 2000) were used in this study. *mee39-1* (SALK_108641) T-DNA mutant was ordered through NASC. Transformation of *pMEE39:MEE39-GFP* into *mee39-1* mutants and *pMEE39:mCherry-N7* into Col-0 plants were performed with floral dip (Clough and Bent, 1998; Hellens *et al*., 2000). Transgenic lines were selected on soil by spraying with 0.1% BASTA for T1 generation. T2 heterozygous *pMEE39:MEE39-GFP* and *pMEE39:mCherry-N7* seedlings were screened for GFP and RFP fluorescence, respectively, to select for homozygous lines. *Mee39-1* mutant was crossed with *mik2*-1 mutant to generate *mee39-1 mik2-1* double mutant. The plants were either grown vertically on 0.9% Difco agar supplemented with non-buffered half strength MS media (pH 5.7) or on soil if not specified. The growth condition followed a 16-h light/8-h dark cycle at 21°C.

*Generation of constructs*

All primers used in PCR are listed in Table S1. To generate *pMEE39:MEE39-GFP*, fragments of *MEE39* promoter, *MEE39* genomic sequence, and *GFP* were amplified by PCR. An 1773 bp promoter was cloned from the upstream region of *MEE39* ORF (AT3G46330), and a flexible alanine linker (GAAAAA) was fused between the *MEE39* genomic sequence and the *GFP* sequence by primer designs. The amplified fragments were cloned into predigested pNEW vector (digested with EcoRI and XbaI) by one-step ligation. To generate *pMEE39:mCherry-N7*, fragments of *MEE39* promoter (same as above), *mCherry*, and the *N7*

nuclear targeting sequence (AT4G19150, Cutler *et al.,* 2000) were amplified by PCR. An alanine linker (GAAAAA) was fused between the *mCherry* and the *N7* sequences by primer designs. The amplified fragments were cloned into predigested pNEW vector (digested with EcoRI and XbaI) by one-step ligation. All the fragments were assembled using NEBuilder® HiFi DNA Assembly Cloning Kit (BioConcept) and following the manufacturer's protocol. The assembled constructs were transformed into DH5α *E. coli* cells and selected by kanamycin resistance. Plasmid DNA extracted from the *E. coli* cells and pSOUP were transformed into electrocompetent GV3101 *Agrobacterium tumefaciens*. The resistant Agrobacterium cells were selected with kanamycin, gentamicin and rifampin. The final Agrobacterium transformants were used for floral dip to generate Arabidopsis transformants.

*Fungal growth strains and culture conditions*

*Fusarium oxysporum* Fo5176 WT and the line expressing *pSIX1:GFP* were used in this study. The cultivation and storage of the strain were performed as described earlier (Di Pietro *et al*, 2001; Kesten *et al.,* 2019; Huerta *et al.,* 2020). In brief, the fungus was grown in liquid potato dextrose broth (PDB) culture at 27°C in the dark for 5 days, and the culture was filtered through miracloth to harvest the spores.

*Generation of pre-germinated Fusarium oxysporum spores*

One mL of 1 x $10^6$ spores were germinated in ½ MS (pH 5.7) + 1% (w/v) sucrose liquid media by shaking overnight at 600 rpm in a 2 mL Eppendorf tube. The germinated spores were centrifuged at 2,000 g for 5 min. Supernatant was discarded and the young hyphae were washed for 3 times with ½ MS liquid media to remove excess sucrose. The fungal culture was then re-suspended to $10^7$ hyphae/mL with ½ MS. This material was used for testing MEE39-GFP and pMEE39:mCherry-N7 using microscopy, and the examination of MEE39-GFP protein levels using Western blot.

*Fusarium oxysporum plate infection assay*

Plants were infected on plates as previously described (Kesten *et al.,* 2019; Huerta *el al.,* 2020). Briefly, seeds were germinated on Whatman filter paper strips in ½ MS media supplemented with 0.9% Agar. At 8 days after germination (dag), the seedlings were transferred to mock or infection plate. The infection plates were prepared by spreading 100 µL 1 x $10^7$ *pSIX1:GFP* spores / mL on the plates. Vascular penetration sites were recorded from 3 to 7 days post treatment (dpt). The vascular penetrations were determined when strong

and linear signals emerged under a Leica M205 FCA fluorescent stereo microscope, which was equipped with a long pass GFP filter (ET GFP LP; Excitation nm: ET480/40x; Emission nm: ET510 LP). The root length was as well recorded during the infection. At 7 dpt, some roots under the mock condition coiled at the bottom of the plates, resulting in an inaccurate observation of root length. Therefore, the root growth (increase of primary root length) was documented from 0 to 6 dpt. The primary root length was measured, and the individual root length reduction was calculated as the following formula to show the level of sensitivity: (mean mock root length $\bar{X}$ - infected root length $_i$) / mean mock root length $\bar{X}$ x 100%.

*Fusarium oxysporum soil infection assay*

Plants were grown on soil with an 8-h light/16-h dark cycles and 65% humidity at 25°C for 21 days and inoculated with Fo5176 spores. Fo5176 spores were prepared as previously described (Huerta *el al.,* 2020). In brief, the fungus was grown in liquid PDB culture at 27°C for 5 days, and the culture was filtered with miracloth to harvest Fo5176 spores. The spores were re-suspended in water and used for inoculation. The plants were gently uprooted and the attached soil was washed off with water. The inoculation was performed by agitating 10 plants in 10 mL 1 x $10^7$ spores / mL at 100 rpm for 10 min. The mock treatment was performed by agitating 10 plants in 10 mL water, at 100 rpm for 10 min. After agitation, the plants were transferred to new pots. Each plant was put into an individual pot, so the space for both the fungal and the plant developments was made even. After 5 dpt, dead plants from the transplant were removed. After 14 dpt, the mock treatments resulted in 100% asymptomatic plants of both the wild type and the mutants. The infected plants were recorded for symptoms and scored on a 1 to 4 scale (1: asymptomatic, 2: ≤ 50% of leaves are wilted, 3: > 50% of leaves are wilted, 4: death).

*Ralstonia solanacearum soil infection assay*

Plants were grown on Jiffy pots with 8-h light/16-h dark cycles and 60% humidity at 22°C for 4 – 5 weeks. The infection assay of *Ralstonia solanacearum* bacteria was performed with the soil-drench method as previously described (Monteiro *et al.,* 2012). In brief, 3 vertical holes were made in Jiffy pots, and the pots were submerged in a solution of overnight-grown *Ralstonia solanacearum* GMI1000 for 30 min. The solution was adjusted to $OD_{600}$ with distilled water, and 30 mL solution was used for each plant. Inoculated plants were then transferred to trays containing a thin layer of soil drenched with the same *Ralstonia solanacearum* solution, and the later growth condition followed 12-h light/12-h dark cycles

and 60% humidity at 27°C. Plant wilting symptoms were recorded and scored. The scoring measured symptoms on a 0 to 4 scale (0: no wilting, 1: 25% wilted leaves, 2: 50% wilted leaves, 3: 75% wilted leaves, and 4 = death).

*Fusarium oxysporum hydroponic infection assay*

The hydroponic infection assay was performed as previously described (Menna *et al*., 2021). The growth condition followed a 16-h light/8-h dark cycle 21°C, and the media was shaken at 80 rpm for growth. Seeds were germinated with liquid ½ MS media supplemented with 1% sucrose. The plants were held by a 2 mm-thick sponge disc and a metal holder in the container, so the rosettes were not submerged in the liquid. After 7 days of germination, the media was changed to ½ MS without sucrose and grown for another 3 days. At 10 dag, the culture was inoculated with a final concentration of 1 x $10^3$ Fo5176 spores / mL and shaken at 100 rpm for 30 min. The culture was changed with fresh ½ MS media and returned to the growth condition. The plant material was then harvested as indicated.

*Subcellular fractionation and organelle proteome immunoisolation*

To detect the proteins enriched in endocytic organelles upon Fo5176 infection, a subcellular fractionation was performed with mock and infected roots. Roots were subjected to hydroponic infection. ≥ 500 mg root tissue was harvested at 2.5 dpt on ice. The sample was ground with a mortar and a pestle in ice-cold homogenization buffer (HB, 8% (w/v) sucrose; 1 mM EDTA; 20 mM HEPES pH 7.5; 20 mM KCl; 1 mM DTT; 0.2% protease inhibitor cocktail (Sigma)) (5 mL/g root FW). Debris was pelleted by centrifugation at 2,500 rpm and 4 °C for 5 min, and the supernatant was further centrifuged at 4,500 rpm and 4°C for 5 min. The following supernatant was again centrifuged at 2,500 rpm and 4°C for 5 min to obtain the postnuclear supernatant (PNS). About 4.5 mL of PNS was loaded on top of a 7 mL 42% (w/v) sucrose cushion and ultra-centrifuged at 40,000 rpm at 2,500 rpm and 4°C for 30 min with an SW-40 rotor (Beckman). The membrane samples were collected from the 8% / 42% (w/v) sucrose interface and used for immunoisolation. The immunoisolation was performed with μMACS GFP Isolation Kit (Miltenyi Biotec). One mL sample was added with 50 μL anti-GFP beads from the kit and incubated at 4 °C for 1 h. The samples were inverted to mix well every 20 min. Microcolumns were prepared by washing once with 200 μL elution buffer (50 mM Tris-HCl pH 8; 150 mM NaCl; 1% Triton X-100) and twice with 200 μL HB buffer. The membrane samples were then loaded into the microcolumns, and washed 5 times with 200 μL HB buffer. The microcolumns were added with 20 μL Laemmli buffer (Laemmli, 1970),

which was preheated to 80°C, and incubated for 5 min. Another 80 µL preheated Laemmli buffer was added to the microcolumns, and the eluate was collected and stored at -20°C until further preparation for MS analysis.

*TCA precipitation, trypsin FASP digestion, and Stage Tip C18 clean-up*

Nine µL cold 100% TCA was added to 80 µL pull-down sample collected as described above. The mixture was vigorously vortexed, briefly spun down, and incubated at 4°C for 30 - 45 min. The sample was centrifuged at 16,000 g and 4°C for 30 min. The supernatant was carefully removed and the pallet was washed/vortexed with 200 µL ice-cold acetone to remove acid. The tube was centrifuged at 16,000 g and 4 °C for 10 min, and the supernatant was removed. The acetone wash was repeated for 3 times, and the sample was air-dried. The following FASP digestion was modified from previous description (Wisniewski et al., 2009). Thirty µL of SDS-lysis buffer (4% (w/v) SDS; 100 mM Tris-HCl pH 8.2; 0.1 M DTT) was added to re-suspend the pellet. The sample was incubated at 700 - 1,000 rpm and 95°C for 5 min, vortexed and spun down briefly. The mixture was then sonicated with 100% amplitude, 70% cycle for 1 min in a VialTweeter powered by UP200St ultrasonic processor (Hielscher Ultrasonics GmbH). The sample was centrifuged at 16,000 g for 10 min, and 1 µL supernatant was take to quantify protein amount with a Qubit (ThermoFisher). Around 40 µg/each sample was determined. The rest of the sample was added with 200 µL UA buffer (8 M urea in 100 mM Tris-HCl pH 8.2) and loaded to a filter unit. The loading was followed with centrifugation at 14,000 g and room temperature (RT) for 20 – 25 min until the entire sample was loaded. The filter unit was added with 200 µL UA buffer and centrifuged at 14,000 g and RT for 20 min and the flow-through was discarded. One hundred µL IAA solution (0.05 M iodoacetamide in UA buffer) was added to the filter unit and mixed at 600 rpm on a thermoblock for 1 min. The sample was incubated for 5 min on the bench and centrifuged at 14,000 g and RT for 12-15 min. The filter unit was washed for 3 times by adding 100 µL UA buffer and centrifuging at 14,000 g and RT for 12-15 min. The filter unit was again washed for twice by adding 100 µL 0.5 M NaCl and centrifuging at 14,000 g and RT for 12-15 min. Trypsin (Promega) was prepared in a 1:50 ratio in TEAB (0.05 M Triethylammoniumbicarbonate pH 8.5). The filter unit was then added with 120 µL trypsin/TEAB and mixed at 600 rpm on a thermoblock for 1 min. The digestion was incubated on the bench for overnight in a wet cell. After incubation, the filter unit was centrifuged at 14,000 g and RT for 15 - 20 min. One hundred µL TEAB was added to the

filter unit, and the unit was centrifuged again at 14,000 g and RT for 5 min. Finally, the eluate was acidified with 5% trifluoroacetic acid (TFA) to final concentration of 0.5% TFA in the sample.

The peptide sample was further cleaned up with in-house made Stage Tip C18 (Rappsilber *et al*., 2007). The Stage Tip was wet by loading 150 µL 100% acetonitrile (ACN) in a 2 mL tube and centrifuged at 2,000 g and RT for 1 min, and the flow-through was discarded. Next, the Stage Tip was equilibrated with 150 µL 60% ACN + 0.1% TFA and centrifuged at 2,000 g and RT for 1 min, and the flow-through was discarded. The Stage Tip was further conditioned by repeating twice of loading 150 µL 3% ACN + 0.1% TFA and centrifuging at 2,000 g and RT for 1 min. After conditioning, the trypsin-digested peptide sample was loaded into the Stage Tip, and the tip was centrifuged at 2,000 g and RT for 2 min. The loading was repeated until the entire sample was loaded. The Stage tip was then washed for 2 – 3 times by adding 150 µL 3% ACN + 0.1% TFA and centrifuging at 2,000 g and RT for 1 min. After washing step, the Stage Tip was placed in a 1.5 mL tube, loaded with 150 µL 60% ACN + 0.1% TFA, and centrifuged at 2,000 g and RT for 2 min. Finally, the eluted sample was completely dried by speed-vacuum and dissolved in 20 µL LC-MS (3% CAN; 0.1% FA) solution for MS analysis.

*LC-MS/MS analysis of proteomes*

The mass spectrometry analysis was performed with the support of Functional Genomics Center Zurich (FGCZ). Dissolved samples were injected by a Waters M-class UPLC system (Waters AG) operating in trap/elute mode. A Symmetry C18 trap column (5 µm, 180 µm X 20 mm, Waters AG) and a HSS T3 C18 reverse-phase column (1.8 µm, 75 µm X 250 mm, Waters AG) as separation column were used. The columns were equilibrated with 99% solvent A (0.1% formic acid (FA) in water) and 1% solvent B (0.1% FA in ACN). Trapping of peptides was performed at 15 µL/min for 30 sec and afterwards the peptides were eluted using the following gradient: 1 - 40% B in 120 min. The flow rate was constant 0.3 µL/min and the temperature was controlled at 50 °C. High accuracy mass spectra were acquired with an Q-Exactive HF mass spectrometer (Thermo Scientific) that was operated in data dependent acquisition mode. A survey scan was followed by up to 12 MS2 scans. The survey scan was recorded using quadrupole transmission in the mass range of 350-1500 m/z with an AGC target of 3E6, a resolution of 120,000 at 200 m/z, and a maximum injection time of 50 ms. All fragment mass spectra were recorded with a resolution of 30,000 at 200 m/z, an AGC target value of 1E5 and a maximum injection time of 50 ms. The normalized collision energy was

set to 28%. Dynamic exclusion was activated and set to 30 s. All recorded data are automatically transferred to a data management system (B-Fabric; Türker *et al*., 2011) and peak lists are extracted automatically using FCC (Barkow-Oesterreicher *et al*., 2013). Peak lists were searched on Mascot server v.2.4.1 (Matrix Science) against Swiss-Prot (all species) database. Tryptic peptides that were permitted with up to 1 possible miscleavages and charge states $2^+$, $3^+$, $4^+$ were allowed in the search. Ccarbamidomethylated cysteine was specified as fixed modification, and oxidized methionine and acetylation at protein N-terminus were specified as variable modifications. Data were searched with a monoisotopic precursor and fragment ions mass tolerance 10 ppm and 0.05 Da, respectively. The search results were then imported into Scaffold v.4 for visualization. A *t*-test analysis on MS2 spectra number was performed to compare the mock treated ones and the inoculated ones of each marker line.

*Confocal microscopy and data processing*

To test the response of MEE39-GFP or *MEE39* promoter activity, 8-day-old roots were inoculated with Fo5176 WT pre-germinated spores (prepared as described above) on ½ MS agar plates or treated with 300 nM isoxaben in 1/2MS liquid media supplemented with 1 % (w/v) sucrose. Media containing the same volume concentration of ethanol were used as the mock treatment of isoxaben.

Root epidermal cells expressing *pMEE39:MEE39-GFP* were imaged with a CSU-W1 Yokogawa spinning disk head fitted to a Nikon Eclipse Ti-E-inverted microscope with a CFI PlanApo × 100 N.A. 1.40 oil immersion objective, two iXon Ultra EM-CCD cameras (Andor, GB), and a ×1.2 lens between the spinning disk and camera was used. GFP was detected using a 488 nm solid-state diode laser and a 525/50 nm emission filter. Time-lapse images were taken with 1 sec intervals for 3 min if not specified. Z-stack analysis was performed by 30 x 0.5 µm sections. The images were processed and analyzed with Fiji (Schindelin *et al*., 2012). Backgrounds were subtracted by the "Subtract Background" tool (rolling ball radius, 20 pixels).

Root epidermal cells expressing *pMEE39:mCherry-N7* were imaged with a Zeiss 780 confocal laser scanning microscope equipped with a 20x 0.5 NA objective. RFP was visualized using 561 nm laser excitation and 592–754 nm spectral detection. Z-stack images were taken, and image tiling and stitching was performed with the ZEN software (Zeiss). The images were further processed and analyzed with Fiji. Frames that had the strongest signal of each cell were selected from the Z-stack, and the mean gray values were measured with the polygon tool.

*Membrane protein isolation and Western blot analysis*

To analyze MEE39-GFP protein levels, membrane proteins were extracted by adapting from a previous method (Abas & Luschnig, 2010). Eight-day-old roots were harvested and ground in liquid nitrogen. To homogenize the samples, 20 mg root tissue was added with 120 µL extraction buffer 1 (50 mM Tris-HCl pH 7.6, 150 mM NaCl, Protease Inhibitor Cocktail pill (PiC 10mg tablet – cOmplete, Roche), 0.5 mM EDTA) on ice. The samples were then centrifuged at 16,250 g and 4°C for 15 min, and the supernatant containing the cytosolic proteins was removed. The pellet, which contained plant debris, unbroken cells, cell wall components, orgenelles, nuclei, and microsomal fractions, was re-suspended with 60 µL extraction buffer 2 (50 mM Tris-HCl pH 7.6, 150 mM NaCl, Protease Inhibitor Cocktail pill, 0.5 mM EDTA, 0.5% Triton-X, 0.5% NP-40) without pipetting. The re-suspended samples were centrifuged at 12,000 g and 4°C for 20 min. The supernatant was collected and quantified for protein concentration with Quick Start Bradford protein assay following the manufacturer's protocol. The samples were then heated in 1x Laemmli buffer at 95°C for 10 min. SDS-PAGE was performed by loading same amount of protein (30 µg/sample) in precast SDS 4 - 12% acrylamide gradient gels (Expedeon, GB). For western blot analysis, nitrocellulose membranes were blocked with 3% non-fat dry milk/0.1 % Tween-20, incubated with the primary antibodies at RT for 2 h (or overnight at 4°C), washed, and incubated with secondary antibodies at RT for 1 h. Primary antibodies are anti-GFP (3H9, 1:1000 dilution, Chromotek) and anti-SYP21 (1:1000 dilution; Tse *et al*., 2004), and they are recognized by the respective secondary antibodies, goat anti-rat HRP (1:5000 dilution; Axon Lab) and goat anti-rabbit HRP (1:5000 dilution; Axon Lab). The protein detection was performed with Westar Supernova kit (Cyanagen), which provides sensitive chemiluminescence detection. The amount of transferred protein was analyzed by incubating the membrane with Ponceau S staining solution (0.1% (w/v) Ponceau S in 5% (v/v) acetic acid) for 10 min and washing with distilled water to remove the background.

*Co-immunoprecipitation analysis*

To detect the possible interactors of MEE39, a co-IP targeting analysis MEE39-GFP was performed, applying Lti6B-GFP co-IP as a negative control. Seven-day old seedlings were grown on hydroponic cultures and subjected to Fo5176 infection as described above for 3 days. The roots were harvested to extract total proteins. 500 mg root tissue was homogenized with a mortar and a pestle on ice in 1 mL extraction buffer (50 mM Tris-HCl pH 8.0, 150 mM

NaCl, 1% Triton-X, 1% (w/v) PVPP, Protease Inhibitor Cocktail pill (PiC 10mg tablet – cOmplete, Roche), 1mM DTT). The samples were centrifuged at 5,000 rpm and 4°C for 5 min, and the supernatant was transferred to a new tube. The samples were centrifuged again at 5,000 rpm and 4°C for 20 min. The supernatant was transferred to a new tube containing 50 µL of anti-GFP µMACS beads (Miltenyi Biotec) and incubated at 4°C for 1 h with rotation. Next, anti-GFP µMACS beads were processed using the µMACS column purification protocol and washed with the wash buffer (50 mM Tris-HCl pH 8.0, 300 mM NaCl, 1% Triton-X, Protease Inhibitor Cocktail pill, 1 mM DTT). Final elution was performed using 80 µl of elution buffer (50 mM Tris-HCl pH 7.5, 2% (w/v) SDS, 1 mM DTT) at 80°C. After elution, samples were stored in -20°C before analyzed with MS.
The isolated proteins were subjected to TCA precipitation, trypsin FASP digestion, Stage Tip C18 clean-up, and LC-MS/MS analysis described above with the support of FGCZ. MS spectra were further analyzed using MaxQuant v.1.1.1.14 software with a peptide FDR of 1% with LFQ intensity quantification (Tyanova *et al*., 2016). The TAIR 10 (www.arabidopsis.org) and SUBA 5 (www.suba.live) databases were used for peptide identification and cellular localization annotation, respectively. LFQ intensities were then analyzed using Perseus software v.1.6.5.0 (Tyanova & Cox, 2018).

*Root growth inhibition assays*
To test the sensibility to isoxaben, plants were grown vertically on 0.9% (w/v) agar supplemented with ½ MS media and 1% (w/v) sucrose (pH 5.7). The growth condition followed a 16-h light/8-h dark cycle at 21°C. At 5 days after germination (dag), the seedlings were transferred to new ½ MS + 1% (w/v) sucrose plates containing either 2 nM isoxaben or ethanol (adjusted to the same volume concentration of isoxaben). At 5 dpt, the primary root length was measured, and the individual root length reduction was calculated as the following formula to show the level of sensitivity: (mean mock root length $\bar{X}$ - treated root length $_i$) / mean mock root length $\bar{X}$ x 100%.
To test the sensibility to SCOOP12 peptides, plants were grown vertically on 0.9% agar supplemented with ½ MS media and 1% sucrose (pH 5.7). The growth condition followed a 16-h light/8-h dark cycle at 21 °C. At 3 dag, the seedlings were transferred to new ½ MS media plates containing 0, 10, 100, or 1000 nM SCOOP12 peptides. At 7 dpt, the primary root length was measured. The root length was normalized to the average mock root length within each genotype to show the root growth inhibition phenotypes.

*RNA extraction and qRT-PCR*

Around 100 mg plant material was harvested and frozen immediately with liquid nitrogen. Eight hundred μL isol-RNA lysis reagent (Lab Force) was added to grind the sample with a pre-chilled mortar and pestle. The homogenate was centrifuged at max speed and 4°C for 10 min. The supernatant was transferred to a new tube and added with 300 μL chloroform. The tube was vortexed strongly for 15 s to be mixed well, and centrifuged at 12,000 g and 4°C for 15 min. The upper phase of the supernatant was carefully transferred to a new tube and added with 500 μL isopropanol and mix well. The tube was incubated at -80°C for 20 min and centrifuged at max speed and 4°C for 20 min. The RNA pellet was washed twice with 80% ethanol and dried at room temperature. The pellet was re-suspended with 20 μL sterile water and measured for concentration with a nanodrop (ThermoFisher). Two μg RNA was then used to synthesize first-strand cDNA using Thermo Scientific MaximaTM H Minus cDNA Synthesis Master Mix with dsDNase (ThermoFisher) following the manufacturer's protocol. The qRT–PCR was performed under the following PCR conditions: 95°C for 3 min, 40 cycles of 94°C for 10 s, 58°C for 15 s, and 72°C for 10 s using Fast SYBR Green Master Mix (ThermoFisher) in a 10 μL reaction. The reference gene GAPDH (At1g13440) was amplified in parallel on each plate for normalization. Fo5176 β-Tubulin (Fo5176.g4360) was used as a reference gene for Fo gene expression. The primers used to amplify target genes are listed in table S2. The $2^{\Delta CT}$ method was used to quantify the relative expression of each gene (Schmittgen & Livak, 2008).

## References

**Abas L, Luschnig C**. **2010**. Maximum yields of microsomal-type membranes from small amounts of plant material without requiring ultracentrifugation. *Analytical Biochemistry* **401**: 217–227.

**Arnaud D, Lee S, Takebayashi Y, Choi D, Choi J, Sakakibara H, Hwang I**. **2017**. Cytokinin-mediated regulation of reactive oxygen species homeostasis modulates stomatal immunity in Arabidopsis. *Plant Cell* **29**: 543–559.

**de Azevedo Souza C, Li S, Lin AZ, Boutrot F, Grossmann G, Zipfel C, Somerville SC**. **2017**. Cellulose-derived oligomers act as damage-associated molecular patterns and trigger defense-like responses. *Plant Physiology* **173**: 2383–2398.

**Bani M, Pérez-de-Luque A, Rubiales D, Rispail N**. **2018**. Physical and chemical barriers in root tissues contribute to quantitative resistance to *Fusarium oxysporum* f. Sp. *pisi* in Pea. *Frontiers in Plant Science* **9**: 199.

**Baral A, Irani NG, Fujimoto M, Nakano A, Mayor S, Mathew MK**. **2015**. Salt-induced remodeling of spatially restricted clathrin-independent endocytic pathways in Arabidopsis root. *Plant Cell* **27**: 1297–1315.

**Barkow-Oesterreicher S, Türker C, Panse C**. **2013**. FCC - An automated rule-based processing tool for life science data. *Source Code for Biology and Medicine* **8**: 3.

**Bischoff V, Cookson SJ, Wu S, Scheible WR**. **2009**. Thaxtomin A affects CESA-complex density, expression of cell wall genes, cell wall composition, and causes ectopic lignification in *Arabidopsis thaliana* seedlings. *Journal of Experimental Botany* **60**: 955–965.

**Brutus A, Sicilia F, Macone A, Cervone F, De Lorenzo G**. **2010**. A domain swap approach reveals a role of the plant wall-associated kinase 1 (WAK1) as a receptor of oligogalacturonides. *Proceedings of the National Academy of Sciences of the United States of America* **107**: 9452–9457.

**Türker, C, Akal F, Schlapbach R**. **2011**. Life sciences data and application integration with B-fabric. *Journal of integrative bioinformatics* **8**: 159.

**Chaudhary A, Chen X, Gao J, Leśniewska B, Hammerl R, Dawid C, Schneitz K**. **2020**. The Arabidopsis receptor kinase STRUBBELIG regulates the response to cellulose deficiency. *PLoS Genetics* **16**: e1008433.

**Chen L, Xiang S, Chen Y, Li D, Yu D**. **2017**. Arabidopsis WRKY45 interacts with the DELLA protein RGL1 to positively regulate age-triggered leaf senescence. *Molecular Plant* **10**: 1174–1189.

**Clough SJ, Bent AF**. **1998**. Floral dip: a simplified method for Agrobacterium-mediated

transformation of *Arabidopsis thaliana*. *Plant Journal* **16**: 735–743.

**Coleman AD, Maroschek J, Raasch L, Takken FLW, Ranf S, Hückelhoven R**. **2021**. The Arabidopsis leucine-rich repeat receptor-like kinase MIK2 is a crucial component of early immune responses to a fungal-derived elicitor. *New Phytologist* **229**: 3453–3466.

**De Coninck B, Timmermans P, Vos C, Cammue BPA, Kazan K**. **2015**. What lies beneath: belowground defense strategies in plants. *Trends in Plant Science* **20**: 91–101.

**Cosgrove DJ**. **2005**. Growth of the plant cell wall. *Nature Reviews Molecular Cell Biology* **6**: 850–861.

**Couto D, Zipfel C**. **2016**. Regulation of pattern recognition receptor signalling in plants. *Nature Reviews Immunology* **16**: 537–552.

**Cutler SR, Ehrhardt DW, Griffitts JS, Somerville CR**. **2000**. Random GFP::cDNA fusions enable visualization of subcellular structures in cells of Arabidopsis at a high frequency. *Proceedings of the National Academy of Sciences of the United States of America* **97**: 3718–3723.

**Czechowski T, Stitt M, Altmann T, Udvardi MK, Scheible WR**. **2005**. Genome-wide identification and testing of superior reference genes for transcript normalization in arabidopsis. *Plant Physiology* **139**: 5–17.

**DeBolt S, Gutierrez R, Ehrhardt DW, Somerville C**. **2007**. Nonmotile cellulose synthase subunits repeatedly accumulate within localized regions at the plasma membrane in arabidopsis hypocotyl cells following 2,6-dichlorobenzonitrile treatment. *Plant Physiology* **145**: 334–338.

**Decreux A, Messiaen J**. **2005**. Wall-associated kinase WAK1 interacts with cell wall pectins in a calcium-induced conformation. *Plant and Cell Physiology* **46**: 268–278.

**Decreux A, Thomas A, Spies B, Brasseur R, Cutsem P Van, Messiaen J**. **2006**. In vitro characterization of the homogalacturonan-binding domain of the wall-associated kinase WAK1 using site-directed mutagenesis. *Phytochemistry* **67**: 1068–1079.

**Desprez T, Juraniec M, Crowell EF, Jouy H, Pochylova Z, Parcy F, Höfte H, Gonneau M, Vernhettes S**. **2007**. Organization of cellulose synthase complexes involved in primary cell wall synthesis in *Arabidopsis thaliana*. *Proceedings of the National Academy of Sciences of the United States of America* **104**: 15572–15577.

**Desprez T, Vernhettes S, Fagard M, Refrégier G, Desnos T, Aletti E, Py N, Pelletier S, Höfte H**. **2002**. Resistance against herbicide isoxaben and cellulose deficiency caused by distinct mutations in same cellulose synthase isoform CESA6. *Plant Physiology* **128**: 482–490.

**Dettmer J, Hong-Hermesdorf A, Stierhof YD, Schumacher K**. **2006**. Vacuolar $H^+$-ATPase activity is required for endocytic and secretory trafficking in Arabidopsis. *Plant Cell* **18**: 715–730.

**Di X, Gomila J, Takken FLW**. **2017**. Involvement of salicylic acid, ethylene and jasmonic acid signalling pathways in the susceptibility of tomato to *Fusarium oxysporum*. *Molecular Plant Pathology* **18**: 1024–1035.

**Di X, Takken FLW, Tintor N**. **2016**. How phytohormones shape interactions between plants and the soil-borne fungus *Fusarium oxysporum*. *Frontiers in Plant Science* **7**: 170.

**Diener AC, Ausubel FM**. **2005**. RESISTANCE TO FUSARIUM OXYSPORUM 1, a dominant Arabidopsis disease-resistance gene, is not race specific. *Genetics* **171**: 305–321.

**Digonnet C, Martinez Y, Denancé N, Chasseray M, Dabos P, Ranocha P, Marco Y, Jauneau A, Goffner D**. **2012**. Deciphering the route of *Ralstonia solanacearum* colonization in *Arabidopsis thaliana* roots during a compatible interaction: Focus at the plant cell wall. *Planta* **236**: 1419–1431.

**Doares SH, Syrovets T, Weiler EW, Ryan CA**. **1995**. Oligogalacturonides and chitosan activate plant defensive genes through the octadecanoid pathway. *Proceedings of the National Academy of Sciences of the United States of America* **92**: 4095–4098.

**Van der Does D, Boutrot F, Engelsdorf T, Rhodes J, McKenna JF, Vernhettes S, Koevoets I, Tintor N, Veerabagu M, Miedes E, *et al.* 2017**. The Arabidopsis leucine-rich repeat receptor kinase MIK2/LRR-KISS connects cell wall integrity sensing, root growth and response to abiotic and biotic stresses. *PLoS Genetics* **13**: e1006832.

**Edel-Hermann V, Lecomte C**. **2019**. Current status of *Fusarium oxysporum* formae speciales and races. *Phytopathology* **109**: 512–530.

**Feng W, Kita D, Peaucelle A, Cartwright HN, Doan V, Duan Q, Liu MC, Maman J, Steinhorst L, Schmitz-Thom I, *et al.* 2018**. The FERONIA Receptor Kinase Maintains Cell-Wall Integrity during Salt Stress through $Ca^{2+}$ Signaling. *Current Biology* **28**: 666-675.e5.

**Fokkens L, Guo L, Dora S, Wang B, Ye K, Sánchez-Rodríguez C, Croll D**. **2020**. A chromosome-Scale genome assembly for the *Fusarium oxysporum* strain Fo5176 to establish a model Arabidopsis-Fungal pathosystem. *G3: Genes, Genomes, Genetics* **10**: 3549–3555.

**Franck CM, Westermann J, Boisson-Dernier A**. **2018**. Plant malectin-like receptor kinases: from cell wall integrity to immunity and beyond. *Annual Review of Plant Biology* **69**: 301–328.

**Gadeyne A, Sánchez-Rodríguez C, Vanneste S, Di Rubbo S, Zauber H, Vanneste K, Van Leene J, De Winne N, Eeckhout D, Persiau G, *et al.* 2014**. The TPLATE adaptor complex

drives clathrin-mediated endocytosis in plants. *Cell* **156**: 691–704.

**Geldner N, Dénervaud-Tendon V, Hyman DL, Mayer U, Stierhof YD, Chory J**. **2009**. Rapid, combinatorial analysis of membrane compartments in intact plants with a multicolor marker set. *Plant Journal* **59**: 169–178.

**Genin S, Denny TP**. **2012**. Pathogenomics of the ralstonia solanacearum species complex. *Annual Review of Phytopathology* **50**: 67–89.

**Gonneau M, Desprez T, Martin M, Doblas VG, Bacete L, Miart F, Sormani R, Hématy K, Renou J, Landrein B, *et al.* 2018**. Receptor kinase THESEUS1 is a rapid alkalinization factor 34 receptor in Arabidopsis. *Current Biology* **28**: 2452-2458.e4.

**Gordon TR**. **2017**. *Fusarium oxysporum* and the Fusarium Wilt Syndrome. *Annual Review of Phytopathology* **55**: 23–39.

**Groen AJ, Sancho-Andrés G, Breckels LM, Gatto L, Aniento F, Lilley KS**. **2014**. Identification of trans-Golgi network proteins in *Arabidopsis thaliana* root tissue. *Journal of Proteome Research* **13**: 763–776.

**Hajný J, Prát T, Rydza N, Rodriguez L, Tan S, Verstraeten I, Domjan D, Mazur E, Smakowska-Luzan E, Smet W, *et al.* 2020**. Receptor kinase module targets PIN-dependent auxin transport during canalization. *Science* **370**: 550–557.

**Haruta M, Sabat G, Stecker K, Minkoff BB, Sussman MR**. **2014**. A peptide hormone and its receptor protein kinase regulate plant cell expansion. *Science* **343**: 408–411.

**He P, Shan L, Lin NC, Martin GB, Kemmerling B, Nürnberger T, Sheen J**. **2006**. Specific bacterial suppressors of MAMP signaling upstream of MAPKKK in Arabidopsis innate immunity. *Cell* **125**: 563–575.

**Hellens RP, Anne Edwards E, Leyland NR, Bean S, Mullineaux PM**. **2000**. pGreen: A versatile and flexible binary Ti vector for Agrobacterium-mediated plant transformation. *Plant Molecular Biology* **42**: 819–832.

**Hématy K, Sado PE, Van Tuinen A, Rochange S, Desnos T, Balzergue S, Pelletier S, Renou JP, Höfte H**. **2007**. A receptor-like kinase mediates the response of Arabidopsis cells to the inhibition of cellulose synthesis. *Current Biology* **17**: 922–931.

**Hok S, Allasia V, Andrio E, Naessens E, Ribes E, Panabières F, Attard A, Ris N, Clément M, Barlet X, *et al.* 2014**. The receptor kinase IMPAIRED OOMYCETE SUSCEPTIBILITY1 attenuates abscisic acid responses in Arabidopsis. *Plant Physiology* **166**: 1506–1518.

**Hok S, Danchin EGJ, Allasia V, Panabières F, Attard A, Keller H**. **2011**. An Arabidopsis (malectin-like) leucine-rich repeat receptor-like kinase contributes to downy mildew disease.

*Plant, Cell and Environment* **34**: 1944–1957.

**Huerta AI, Kesten C, Menna AL, Sancho-Andrés G, Sanchez-Rodriguez C**. **2020**. In-plate quantitative characterization of *Arabidopsis thaliana* susceptibility to the fungal vascular pathogen *Fusarium oxysporum. Current Protocols in Plant Biology* **5**: e20113.

**Karimi M, De Meyer B, Hilson P**. **2005**. Modular cloning in plant cells. *Trends in Plant Science* **10**: 103–105.

**Kesten C, Gámez-Arjona FM, Menna A, Scholl S, Dora S, Huerta AI, Huang H, Tintor N, Kinoshita T, Rep M, *et al.* 2019**. Pathogen-induced pH changes regulate the growth-defense balance in plants . *The EMBO Journal* **38**: e101822.

**Kesten C, Menna A, Sánchez-Rodríguez C**. **2017**. Regulation of cellulose synthesis in response to stress. *Current Opinion in Plant Biology* **40**: 106–113.

**Ben Khaled S, Postma J, Robatzek S**. **2015**. A moving view: subcellular trafficking processes in pattern recognition receptor triggered plant immunity. *Annual Review of Phytopathology* **53**: 379–402.

**Kohorn BD, Johansen S, Shishido A, Todorova T, Martinez R, Defeo E, Obregon P**. **2009**. Pectin activation of MAP kinase and gene expression is WAK2 dependent. *Plant Journal* **60**: 974–982.

**Kubicek CP, Starr TL, Glass NL**. **2014**. Plant cell wall-degrading enzymes and their secretion in plant-pathogenic fungi. *Annual Review of Phytopathology* **52**: 427–451.

**Laemmli UK**. **1970**. Cleavage of structural proteins during the assembly of the head of bacteriophage T4. *Nature* **227**: 680–685.

**Lionetti V, Métraux JP**. **2014**. Plant cell wall in pathogenesis, parasitism and symbiosis. *Frontiers in Plant Science* **5**: 612.

**Lyons R, Stiller J, Powell J, Rusu A, Manners JM, Kazan K**. **2015**. *Fusarium oxysporum* triggers tissue-specific transcriptional reprogramming in *Arabidopsis thaliana*. *PLoS ONE* **10**: e0121902.

**Ma X, Xu G, He P, Shan L**. **2016**. SERKing coreceptors for receptors. *Trends in Plant Science* **21**: 1017–1033.

**Masachis S, Segorbe D, Turrà D, Leon-Ruiz M, Fürst U, El Ghalid M, Leonard G, López-Berges MS, Richards TA, Felix G, *et al.* 2016**. A fungal pathogen secretes plant alkalinizing peptides to increase infection. *Nature Microbiology* **1**: 1–9.

**Menna A, Dora S, Sancho-Andrés G, Kashyap A, Gasperini D, Coll NS, Sánchez-Rodríguez C.** 2021. A primary cell wall cellulose-dependent defense mechanism against vascular pathogens revealed by time-resolved dual-transcriptomics. *BMC Biology* **In press**.

**Miao Y, Zentgraf U**. **2007**. The antagonist function of Arabidopsis WRKY53 and ESR/ESP in leaf senescence is modulated by the jasmonic and salicylic acid equilibrium. *Plant Cell* **19**: 819–830.

**Michielse CB, Rep M**. **2009**. Pathogen profile update: *Fusarium oxysporum*. *Molecular Plant Pathology* **10**: 311–324.

**Monteiro F, Solé M, Van Dijk I, Valls M**. **2012**. A chromosomal insertion toolbox for promoter probing, mutant complementation, and pathogenicity studies in *Ralstonia solanacearum*. *Molecular Plant-Microbe Interactions* **25**: 557–568.

**Pagnussat GC, Yu HJ, Ngo QA, Rajani S, Mayalagu S, Johnson CS, Capron A, Xie LF, Ye D, Sundaresan V**. **2005**. Genetic and molecular identification of genes required for female gametophyte development and function in Arabidopsis. *Development* **132**: 603–614.

**Di Pietro A, García-Maceira FI, Méglecz E, Roncero MIG**. **2004**. A MAP kinase of the vascular wilt fungus *Fusarium oxysporum* is essential for root penetration and pathogenesis. *Molecular Microbiology* **39**: 1140–1152.

**Rappsilber J, Mann M, Ishihama Y**. **2007**. Protocol for micro-purification, enrichment, pre-fractionation and storage of peptides for proteomics using StageTips. *Nature Protocols* **2**: 1896–1906.

**Rhodes J, Yang H, Moussu S, Boutrot F, Santiago J, Zipfel C**. **2021**. Perception of a divergent family of phytocytokines by the Arabidopsis receptor kinase MIK2. *Nature Communications* **12**: 1–10.

**Robinson DG, Jiang L, Schumacher K**. **2008**. The endosomal system of plants: charting new and familiar territories. *Plant Physiology* **147**: 1482–1492.

**Rui Y, Dinneny JR**. **2020**. A wall with integrity: surveillance and maintenance of the plant cell wall under stress. *New Phytologist* **225**: 1428–1439.

**Schallus T, Jaeckh C, Fehér K, Palma AS, Liu Y, Simpson JC, Mackeen M, Stier G, Gibson TJ, Feizi T, *et al.* 2008**. Malectin: A novel carbohydrate-binding protein of the endoplasmic reticulum and a candidate player in the early steps of protein N-glycosylation. *Molecular Biology of the Cell* **19**: 3404–3414.

**Schindelin J, Arganda-Carreras I, Frise E, Kaynig V, Longair M, Pietzsch T, Preibisch S, Rueden C, Saalfeld S, Schmid B, *et al.* 2012**. Fiji: An open-source platform for biological-image analysis. *Nature Methods* **9**: 676–682.

**Schmittgen TD, Livak KJ**. **2008**. Analyzing real-time PCR data by the comparative CT method. *Nature Protocols* **3**: 1101–1108.

**Schwihla M, Korbei B**. **2020**. The beginning of the end: initial steps in the degradation of

plasma membrane proteins. *Frontiers in Plant Science* **11**: 680.

**Singh SK, Fischer U, Singh M, Grebe M, Marchant A**. **2008**. Insight into the early steps of root hair formation revealed by the procuste1 cellulose synthase mutant of *Arabidopsis thaliana*. *BMC Plant Biology* **8**: 1–12.

**Smakowska-Luzan E, Mott GA, Parys K, Stegmann M, Howton TC, Layeghifard M, Neuhold J, Lehner A, Kong J, Grünwald K, *et al.* 2018**. An extracellular network of Arabidopsis leucine-rich repeat receptor kinases. *Nature* **553**: 342–346.

**Sørensen I, Willats WGT**. **2011**. Screening and characterization of plant cell walls using carbohydrate microarrays. *Methods in molecular biology (Clifton, N.J.)* **715**: 115–121.

**Stegmann M, Monaghan J, Smakowska-Luzan E, Rovenich H, Lehner A, Holton N, Belkhadir Y, Zipfel C**. **2017**. The receptor kinase FER is a RALF-regulated scaffold controlling plant immune signaling. *Science* **355**: 287–289.

**Tinevez JY, Perry N, Schindelin J, Hoopes GM, Reynolds GD, Laplantine E, Bednarek SY, Shorte SL, Eliceiri KW**. **2017**. TrackMate: An open and extensible platform for single-particle tracking. *Methods* **115**: 80–90.

**Tse YC, Mo B, Hillmer S, Zhao M, Lo SW, Robinson DG, Jiang L**. **2004**. Identification of multivesicular bodies as prevacuolar compartments in *Nicotiana tabacum* BY-2 cells. *Plant Cell* **16**: 672–693.

**Tyanova S, Cox J**. **2018**. Perseus: A bioinformatics platform for integrative analysis of proteomics data in cancer research. *Methods in Molecular Biology* **1711**: 133–148.

**Tyanova S, Temu T, Cox J**. **2016**. The MaxQuant computational platform for mass spectrometry-based shotgun proteomics. *Nature Protocols* **11**: 2301–2319.

**Wagner TA, Kohorn BD**. **2001**. Wall-associated kinases are expressed throughout plant development and are required for cell expansion. *Plant Cell* **13**: 303–318.

**Wiśniewski JR, Zougman A, Nagaraj N, Mann M**. **2009**. Universal sample preparation method for proteome analysis. *Nature Methods* **6**: 359–362.

**Wolf S**. **2017**. Plant cell wall signalling and receptor-like kinases. *Biochemical Journal* **474**: 471–492.

**Xiao Y, Stegmann M, Han Z, DeFalco TA, Parys K, Xu L, Belkhadir Y, Zipfel C, Chai J**. **2019**. Mechanisms of RALF peptide perception by a heterotypic receptor complex. *Nature* **572**: 270–274.

**Xu SL, Rahman A, Baskin TI, Kieber JJ**. **2008**. Two leucine-rich repeat receptor kinases mediate signaling, linking cell wall biosynthesis and ACC synthase in Arabidopsis. *Plant Cell* **20**: 3065–3079.

**Yuan N, Yuan S, Li Z, Zhou M, Wu P, Hu Q, Mendu V, Wang L, Luo H**. **2018**. STRESS INDUCED FACTOR 2, a leucine-rich repeat kinase regulates basal plant pathogen defense. *Plant Physiology* **176**: 3062–3080.

**Zentgraf U, Doll J**. **2019**. Arabidopsis WRKY53, a node of multi-layer regulation in the network of senescence. *Plants* **8**: 578.

## Supplemental Figures

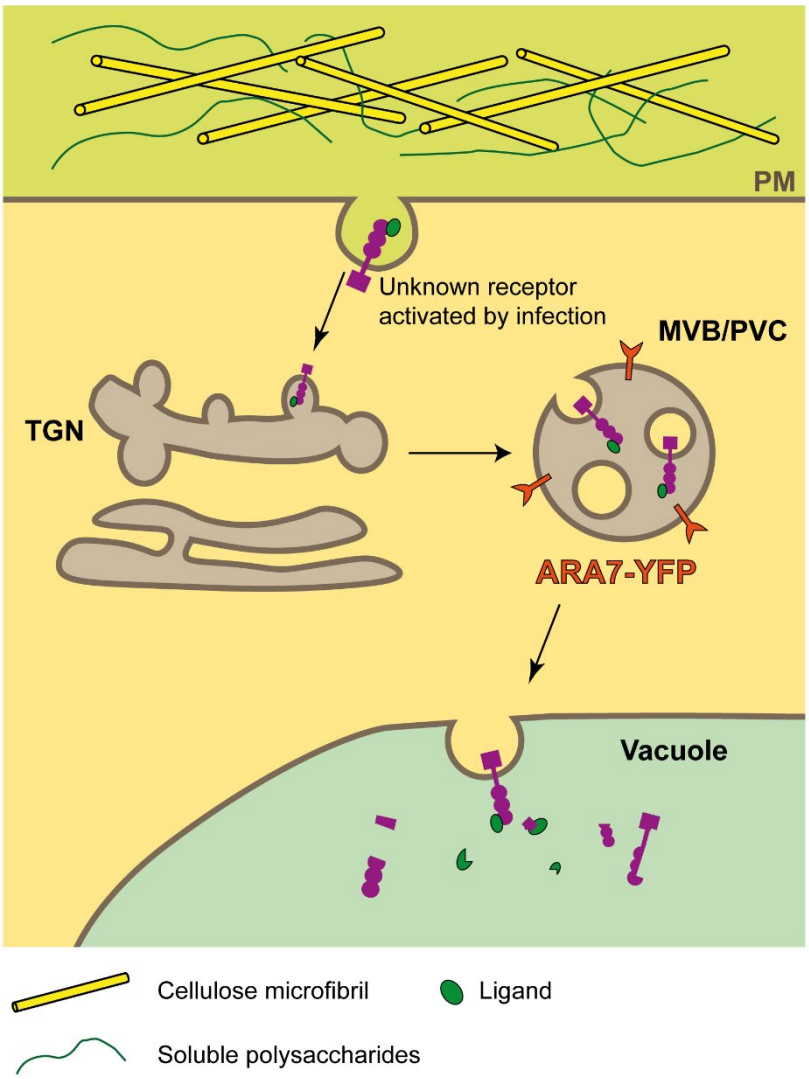


**Figure S1. Illustration of the strategy to identify new plant receptors involved in defense to Fo5176.** After ligand perception, plasma membrane (PM) receptors are internalized by endocytosis and transported through the trans-Golgi network (TGN) and the Multivesicular body/Prevacuolar compartment (MVB/PVC) for vacuolar degradation. PM proteins involved in Arabidopsis-Fo interaction should be enriched in the MVB/PVC when plants are infected by the fungus. The MVB/PVC marker line ARA7-YFP was utilized to immunoprecipitate proteins located in the MVB/PVC. The black arrows indicate the canonical endocytic pathway towards the vacuole.

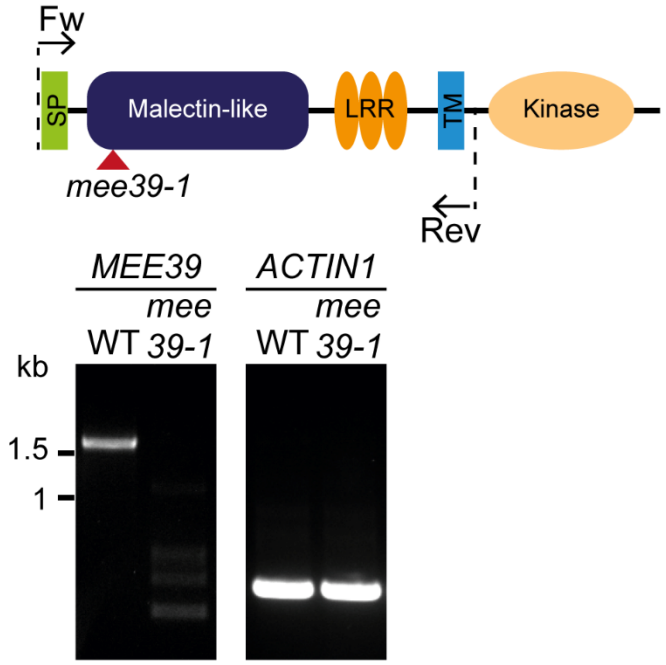


**Figure S2. *mee39-1* mutant carries a knock-out mutation in *MEE39*.** Two-week-old WT and *mee39-1* roots were used to extract RNA and synthesize cDNA for RT-PCR analysis of *MEE39*. The protein structure of MEE39 is depicted in the upper panel. A red arrowhead indicates the T-DNA insertion in *mee39-1* affecting the corresponding protein domains. The primer pair used in RT-PCR to detect *MEE39* transcript is indicated by the black arrows and dashed lines. The agarose gel electrophoresis analysis of RT-PCR products is displayed in the lower panel. *ACTIN1* transcripts were detected in both WT and *mee39-1* as a positive control. Three biological replicates were performed with the same results. A representative replicate is shown.

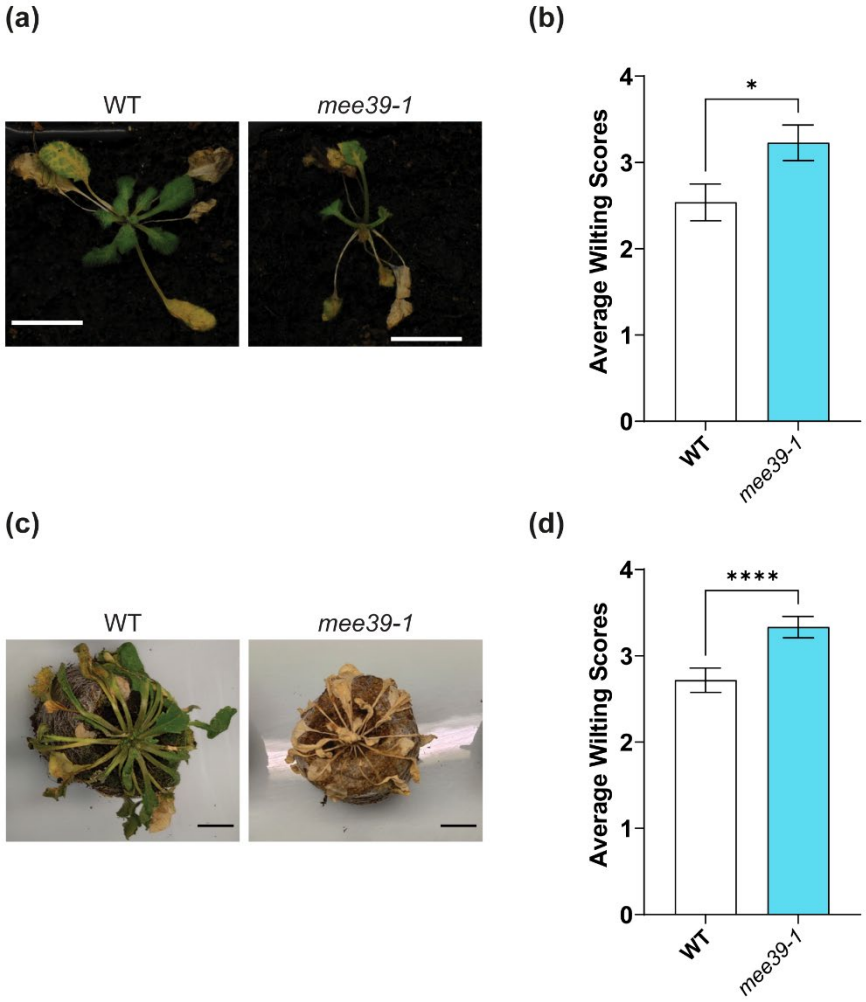


**Figure S3. *mee39-1* mutant is more susceptible than wild-type plants to both *Fusarium oxysporum* and *Ralstonia solanacearum* infection in soil.** (a) Representative aboveground phenotype of WT and *mee39-1* plants at 14 dpt with Fo5176 spores . Scale bars = 1 cm. (b) Wilt disease symptom scoring of plants depicted in (a). The symptoms were scored on the scale of 1 to 4 (1: asymptomatic, 2: ≤ 50% of leaves are wilted, 3: > 50% of leaves are wilted, 4: death). $N \geq 35$ plants were obtained from 2 experiments (≥ 15 plants/experiments were used). Values are Av ± SE. (c) Representative aboveground phenotype of WT and *mee39-1* plants 18 dpt with *Ralstonia solanacearum*. Scale bars = 1 cm. (d) Wilt disease symptom scoring of plants depicted in (c). The symptoms were scored on the scale of 0 to 4 (0: asymptomatic, 1: 25% wilted leaves, 2: 50% wilted leaves, 3: 75% wilted leaves, 4: death). $N \geq 74$ plants were obtained from 3 experiments (≥ 24 plants/experiments were used). Values are Av ± SE. In (b) and (d), data were analyzed by *t-test*; $*P < 0.05$; **** $P \leq 0.0001$.

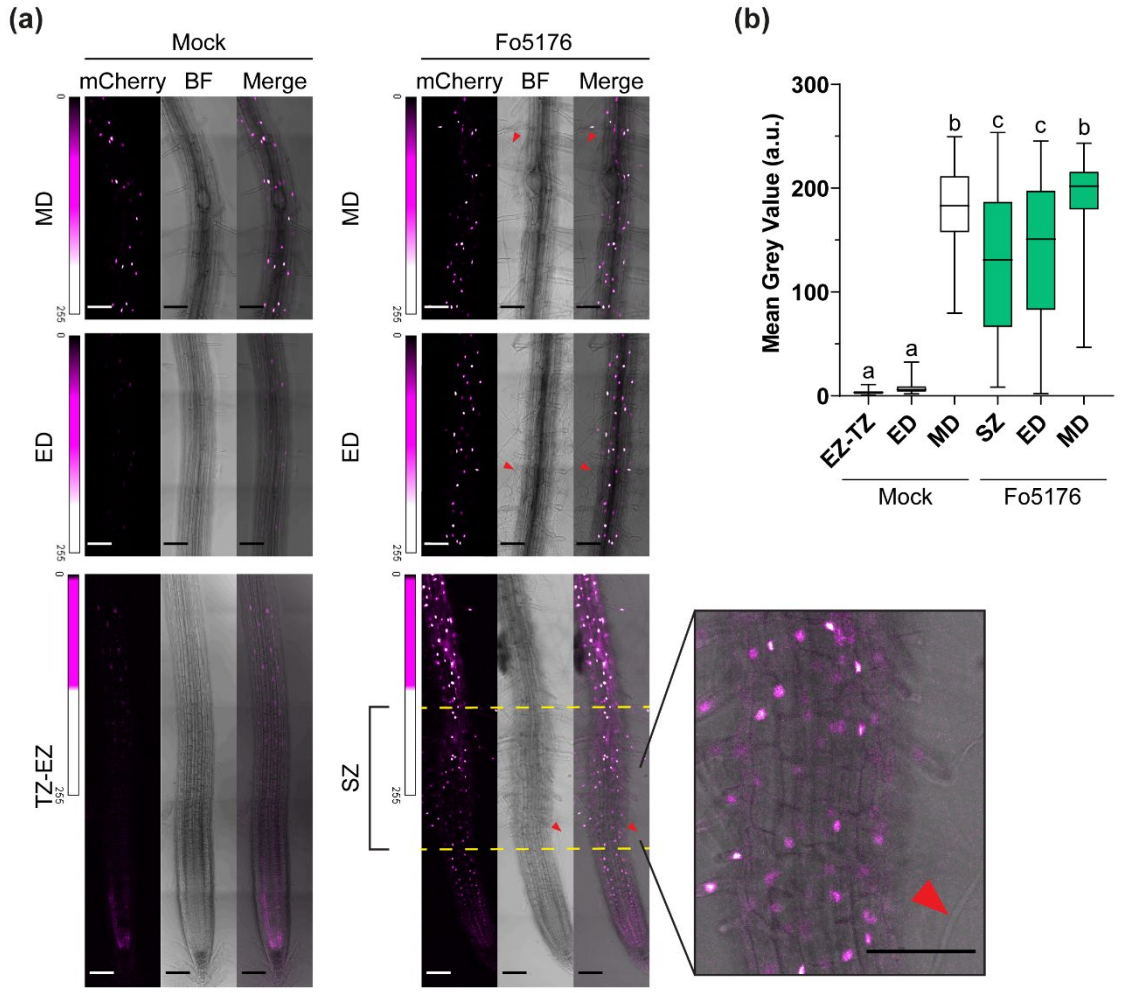


**Figure S4. *MEE39* promoter remains activated by Fo5176 at 3 dpt.** (a) Representative confocal images of 8-day-old root epidermal cells expressing *pMEE39:mCherry-N7* after 3-day exposure of pre-germinated Fo5176 spores. mCherry signal intensities are displayed as the relative heatmaps. BF, brightfield. TZ-EZ, transition zone to elongation zone. ED, early differentiation zone. MD, middle differentiation zone. Red arrowheads indicate fungal hyphae. Scale bars = 100 μm. (b) Quantification of the mCherry signal intensity at different root developmental zones after Fo5176 hyphae contact as depicted in (a). $N \geq 100$ cells were obtained from 3 experiments (≥ 6 cells/root and 3 roots/experiment were imaged). Box plots: centerlines show the medians; box limits indicate the 25th and 75th percentiles; whiskers extend to the minimum and maximum. Data were analyzed by one-way ANOVA followed by Dunn's multiple comparisons test. Alphabet letters indicate significant differences with $P < 0.05$.

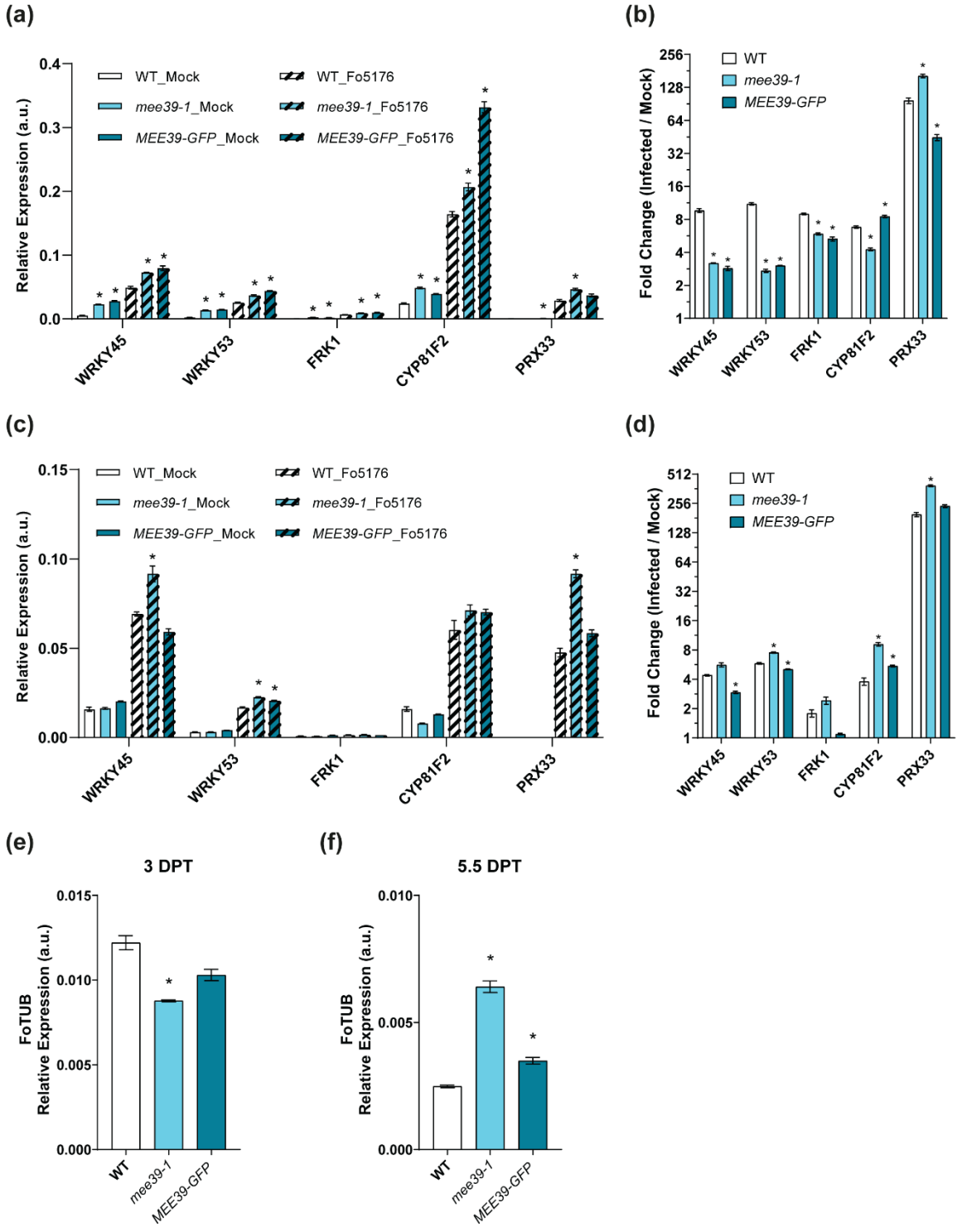


**Figure S5. Immunity marker gene expressions are activated later in *mee39-1* compared to the WT by Fo5176 infection.** (a) and (c) Immunity marker gene expressions relative to *AtGAPDH* in WT, *mee39-1*, and *MEE39-1* at 3 dpt (a) or 5.5 dpt (c) with mock or exposure to Fo5176 *pSIX1:GFP* spores on plates. (b) and (d) Levels of immunity marker gene activation upon Fo5176 at 3 dpt (b) or 5.5 dpt (d) analyzed by normalizing to the mock (ΔΔCt method). The y-axes are scaled by Log 2. (e) and (f) Fo5176 *TUB* expression relative to *AtGAPDH* in WT, *mee39-1*, and *MEE39-1* at 3 or 5.5 dpt with exposure to Fo5176 *pSIX1:GFP* spores on plates. Three experiments were performed with similar trends, and a representative experiment is shown. $N = 3$ technical replicates from ≥ 20 roots. Values

are Av ± SE. Data were analyzed by one-way ANOVA followed by Dunnett's T3 multiple comparisons test. Asterisk indicates the difference from the WT with $P < 0.05$.

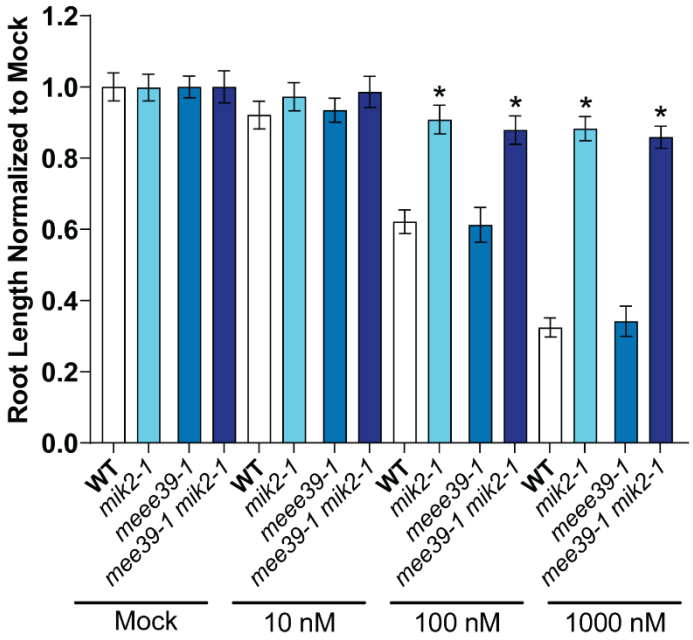


**Figure S6. *mee39-1* mutant is as sensitive as wild-type plants to SCOOP12.** Three-day-old seedlings were treated with 10, 100, and 1000 nM SCOOP12 peptides on plates for 7 days, and the primary root length was measured. The root length was normalized to the average mock root length within each genotypes. Two experiments were performed with similar results, and a representative experiment is shown. $N = 12$ roots were used in one experiment. Values are Av ± SE. Data were analyzed by one-way ANOVA followed by Dunnett's multiple comparisons test comparing to the WT under each condition. *$P < 0.05$.

**Table S1. MEE39 is only found in Brassicales.** Lineage Report is generated from NCBI (https://blast.ncbi.nlm.nih.gov/Blast.cgi) BLAST search of MEE39 protein sequence against non-redundant protein sequences database of green plants. The Score column lists the highest bit score from that group. The bit score measures sequence similarity independent of query sequence length and database size and is normalized based on the raw pairwise alignment score.

| Organism | Blast Name | Score | Number of Hits |
|---|---|---|---|
| Brassicales | eudicots | | 125 |
| .Brassicaceae | eudicots | | 124 |
| ..Camelineae | eudicots | | 59 |
| ...Arabidopsis | eudicots | | 34 |
| ....Arabidopsis thaliana | eudicots | 1823 | 27 |
| ....Arabidopsis lyrata subsp. lyrata | eudicots | 1667 | 6 |
| ....Arabidopsis arenosa | eudicots | 1117 | 1 |
| ...Camelina sativa | eudicots | 1595 | 13 |
| ...Capsella rubella | eudicots | 1582 | 12 |
| ..Brassica rapa | eudicots | 1447 | 14 |
| ..Brassica napus | eudicots | 1429 | 12 |
| ..Sinapis alba | eudicots | 1394 | 4 |
| ..Brassica rapa subsp. trilocularis | eudicots | 1379 | 2 |
| ..Eutrema salsugineum | eudicots | 1236 | 10 |
| ..Microthlaspi erraticum | eudicots | 1177 | 2 |
| ..Brassica oleracea var. oleracea | eudicots | 1076 | 5 |
| ..Arabis nemorensis | eudicots | 1067 | 3 |
| ..Brassica cretica | eudicots | 1066 | 2 |
| ..Raphanus sativus | eudicots | 1066 | 7 |
| ..Brassica oleracea | eudicots | 1064 | 3 |
| ..Brassica carinata | eudicots | 1048 | 1 |
| .Tarenaya hassleriana | eudicots | 1046 | 1 |

**Table S2. Primers used in this study.**

| Name | Sequence (5' → 3') | Use |
|---|---|---|
| SALK_108641 LP | CAAACTTTCTAGATGCGCCAG | Genotyping *mee39-1* |
| SALK_108641 RP | GGCGAATGATACTTACATCGC | |
| SALK_LBb1 | CGCTTTCTTCCCTTCCTTTCTC | |
| pNew_EcoRI_pMEE39_Fw | CGAATTGGAGCTGCGGCCGCGAATTCATCCTCTTACTTTCCAAGCAAAATCAAGA | Cloning *pMEE39:MEE39-GFP* *pMEE39:mCherry-N7* |
| pNew_pMEE39_Rev | GATTCCTCCGATCACAATACACGC | Cloning *pMEE39:MEE39-GFP* |
| gMEE39_Fw | GTATTGTGATCGGAGGAATCATGAAGAATCTTTGTTGGGTTTTTCTGTC | |
| gMEE39_Ala_Rev | CGCCGCTGCTGCGGCGCCTCTTGCCTTAGGCTTCACATCAGTATC | |
| Ala_GFP_Fw | GGCGCCGCAGCAGCGGCGATGGTGAGCAAGGGCGAGG | |
| GFP_Xbal_Rev | TTTCATCTTCATCTTCATATTCTAGATTACTTGTACAGCTCGTCCATGCCG | |
| pMEE39_mCh_Rev | CCTCGCCCTTGCTCACCATGATTCCTCCGATCACAATACACGC | Cloning *pMEE39:mCherry-N7* |
| mCh_Fw | ATGGTGAGCAAGGGCGAGG | |
| mCh_Ala_Rev | GGCGCCCGCCGCCGCCGCCGCTCCCTTGTACAGCTCGTCCATGCC | |
| Ala_Fw | GGAGCGGCGGCGG | |
| N7_XbaI_Rev | TTTCATCTTCATCTTCATATTCTAGATCACTCTTCTTCTTGATCAGCTTCTGTGTCG | |
| MEE39_RT_Fw | ATGAAGAATCTTTGTTGGGTTTTTCTGTC | Examining the knock-out mutation in *mee39-1* (*ACTIN1*, At2g37620, was used as a control) |
| MEE39_RT_Rev | CCACGGTTCAGGTTTATTTCTTG | |
| ACTIN1_RT_Fw | TGGTTGGGATGGGGCAAAAG | |
| ACTIN1_RT_Rev | ATTTCACGCTCTGCTGTGGTGG | |
| FoTUB_Fw | AACTCCGATGAGACCTTCTG | qRT-PCR (Kesten *et al*., 2019) |
| FoTUB_Rev | GACATGACAGCAGAAACGAG | |
| WRKY45_Fw | GAACAATCCATTCCCCAGGAG | qRT-PCR (de Azevedo Souza *et al*., 2017) |
| WRKY45_Rev | GGAGGGAAGATGTGCATTTGTG | |
| WRKY53_Fw | GCGACAAGACACCAGAGTCA | qRT-PCR (Masachis *et al*., 2016) |
| WRKY53_Rev | ACCGTTGGATTGAACCAGTC | |
| FRK1_Fw | TGCAGCGCAAGGACTAGAG | qRT-PCR (Van der Does *et al*., 2017) |
| FRK1_Rev | ATCTTCGCTTGGAGCTTCTC | |
| CYP81F2_Fw | AATGGAGAGAGCAACACAATG | |
| CYP81F2_Rev | ATACTGAGCATGAGCCCTTTG | |
| PRX33_FW | ATCGTCCTTCTGATCTTGTTGCG | qRT-PCR (Arnaud *et al*., 2017) |
| PRX33_Rev | GCAGATCGAAATCCACTAAGACG | |
| MEE39_Fw | CATCGAGTGGCTTGAGTGGG | qRT-PCR |
| MEE39_Rev | TAGTGGCTAGAAACTCGGGC | |
| GAPDH 600b_Fw | AGGTGGAAGAGCTGCTTCCTTC | qRT-PCR (Czechowski *et al*., 2005) |
| GAPDH 600b_Rev | GCAACACTTTCCCAACAGCCT | |

**Appendix I. Differential MS2 spectra detection in organelle-IP upon Fo5176 infection.**
The MS2 spectra detected from four (1-4) experiments of mock (m) and infected (i) samples are shown.

| ARA7-YFP IP profile | | | | | | | | | | | |
|---|---|---|---|---|---|---|---|---|---|---|---|
| | | | | MS2 spectra count | | | | | | | |
| Description | Accession Number | t-test (p-value) | Fold Change by Category (Infected/mock) | ARA7-YFP_m_1 | ARA7-YFP_m_2 | ARA7-YFP_m_3 | ARA7-YFP_m_4 | ARA7-YFP_i_1 | ARA7-YFP_i_2 | ARA7-YFP_i_3 | ARA7-YFP_i_4 |
| Probable boron transporter 2 OS=Arabidopsis thaliana GN=BOR2 PE=2 SV=1 | sp\|Q9M1P7\|BOR2_ARATH | 0.00054 | 0 | 1 | 1 | 2 | 1 | 0 | 0 | 0 | 0 |
| Cluster of Auxin efflux carrier component 3 OS=Arabidopsis thaliana GN=PIN3 PE=1 SV=1 (sp\|Q9S7Z8\|PIN3_ARATH) | sp\|Q9S7Z8\|PIN3_ARATH [3] | 0.026 | 0 | 3 | 1 | 5 | 1 | 0 | 0 | 0 | 0 |
| Fasciclin-like arabinogalactan protein 9 OS=Arabidopsis thaliana GN=FLA9 PE=1 SV=1 | sp\|Q9ZWA8\|FLA9_ARATH | 0.041 | 0 | 1 | 0 | 2 | 1 | 0 | 0 | 0 | 0 |
| Vesicle-associated protein 2-2 OS=Arabidopsis thaliana GN=PVA22 PE=1 SV=1 | sp\|B9DHD7\|VAP22_ARATH | 0.014 | 0.06 | 3 | 1 | 5 | 2 | 0 | 1 | 0 | 0 |
| Marneral synthase OS=Arabidopsis thaliana GN=MRN1 PE=1 SV=1 | sp\|Q9FJV8\|PEN5_ARATH | 0.032 | 0.06 | 11 | 10 | 11 | 0 | 0 | 1 | 1 | 0 |
| Probable cysteine proteinase At4g11320 OS=Arabidopsis thaliana GN=At4g11320 PE=2 SV=1 | sp\|Q9SUS9\|CPR4_ARATH | 0.027 | 0.08 | 16 | 12 | 16 | 1 | 0 | 1 | 1 | 1 |
| 24-methylenesterol C-methyltransferase 3 OS=Arabidopsis thaliana GN=SMT3 PE=2 SV=1 | sp\|Q94JS4\|SMT3B_ARATH | 0.0054 | 0.2 | 11 | 7 | 11 | 5 | 3 | 1 | 3 | 0 |
| Cytochrome P450 71A16 OS=Arabidopsis thaliana GN=CYP71A16 PE=2 SV=1 | sp\|Q9FH66\|C71AG_ARATH | 0.034 | 0.2 | 24 | 10 | 21 | 6 | 4 | 6 | 0 | 1 |
| ABC transporter G family member 14 OS=Arabidopsis thaliana GN=ABCG14 PE=2 SV=1 | sp\|Q9C6W5\|AB14G_ARATH | 0.046 | 0.2 | 3 | 1 | 4 | 1 | 0 | 1 | 0 | 0 |
| Translocon-associated protein subunit alpha OS=Arabidopsis thaliana GN=At2g21160 PE=2 SV=3 | sp\|P45434\|SSRA_ARATH | 0.003 | 0.3 | 4 | 5 | 5 | 5 | 3 | 2 | 1 | 0 |
| Beta-1,3-galactosyltransferase 7 OS=Arabidopsis thaliana GN=B3GALT7 PE=2 SV=1 | sp\|Q6NQB7\|B3GT7_ARATH | 0.023 | 0.3 | 2 | 2 | 1 | 2 | 1 | 0 | 0 | 1 |
| 24-methylenesterol C-methyltransferase 2 OS=Arabidopsis thaliana GN=SMT2 PE=1 SV=2 | sp\|Q39227\|SMT2_ARATH | 0.03 | 0.3 | 10 | 6 | 17 | 6 | 3 | 3 | 2 | 2 |
| THO complex subunit 3 OS=Arabidopsis thaliana GN=THO3 PE=1 SV=1 | sp\|Q9FKT5\|THOC3_ARATH | 0.049 | 0.3 | 1 | 1 | 1 | 2 | 1 | 1 | 0 | 0 |
| NADPH--cytochrome P450 reductase 1 OS=Arabidopsis thaliana GN=ATR1 PE=1 SV=1 | sp\|Q9SB48\|NCPR1_ARATH | 0.031 | 0.4 | 16 | 8 | 22 | 14 | 9 | 8 | 6 | 2 |
| Cluster of Endoglucanase 25 OS=Arabidopsis thaliana GN=KOR PE=1 SV=1 (sp\|Q38890\|GUN25_ARATH) | sp\|Q38890\|GUN25_ARATH [2] | 0.042 | 0.4 | 6 | 5 | 4 | 3 | 2 | 4 | 2 | 0 |
| Syntaxin-22 OS=Arabidopsis thaliana GN=SYP22 PE=1 SV=1 | sp\|P93654\|SYP22_ARATH | 0.042 | 0.4 | 3 | 2 | 4 | 2 | 2 | 2 | 1 | 0 |
| Very-long-chain (3R)-3-hydroxyacyl-[acyl-carrier protein] dehydratase PASTICCINO 2 OS=Arabidopsis thaliana GN=PAS2 PE=1 SV=1 | sp\|Q8VZB2\|PAS2_ARATH | 0.01 | 0.5 | 4 | 6 | 4 | 3 | 2 | 1 | 2 | 2 |
| Apyrase 2 OS=Arabidopsis thaliana GN=APY2 PE=1 SV=1 | sp\|Q9SPM5\|APY2_ARATH | 0.016 | 0.5 | 7 | 5 | 9 | 7 | 5 | 4 | 2 | 2 |
| Probable methyltransferase PMT21 OS=Arabidopsis thaliana GN=ERD3 PE=2 SV=1 | sp\|Q94II3\|PMTL_ARATH | 0.026 | 0.5 | 17 | 13 | 15 | 7 | 4 | 5 | 10 | 6 |
| Cluster of Cellulose synthase A catalytic subunit 1 [UDP-forming] OS=Arabidopsis thaliana GN=CESA1 PE=1 SV=1 (sp\|O48946\|CESA1_ARATH) | sp\|O48946\|CESA1_ARATH [3] | 0.027 | 0.5 | 20 | 14 | 24 | 15 | 6 | 6 | 13 | 13 |
| Probable methyltransferase PMT24 OS=Arabidopsis thaliana GN=At1g29470 PE=2 SV=1 | sp\|Q6NPR7\|PMTO_ARATH | 0.029 | 0.5 | 23 | 19 | 33 | 17 | 15 | 13 | 12 | 11 |
| Protein NRT1/ PTR FAMILY 6.3 OS=Arabidopsis thaliana GN=NPF6.3 PE=1 SV=1 | sp\|Q05085\|PTR7_ARATH | 0.029 | 0.5 | 3 | 5 | 4 | 2 | 2 | 1 | 1 | 2 |
| Cluster of Cellulose synthase A catalytic subunit 3 [UDP-forming] OS=Arabidopsis thaliana GN=CESA3 PE=1 SV=2 (sp\|Q941L0\|CESA3_ARATH) | sp\|Q941L0\|CESA3_ARATH [3] | 0.034 | 0.5 | 29 | 36 | 32 | 16 | 12 | 10 | 15 | 21 |
| Membrane steroid-binding protein 2 OS=Arabidopsis thaliana GN=MSBP2 PE=1 SV=1 | sp\|Q9M2Z4\|MSBP2_ARATH | 0.043 | 0.5 | 4 | 7 | 4 | 5 | 3 | 1 | 4 | 1 |
| Synaptotagmin-5 OS=Arabidopsis thaliana GN=SYT5 PE=2 SV=1 | sp\|Q8L706\|SYT5_ARATH | 0.026 | 0.6 | 7 | 13 | 10 | 9 | 6 | 6 | 6 | 6 |
| Cluster of Calcium-transporting ATPase 1, endoplasmic reticulum-type OS=Arabidopsis thaliana GN=ECA1 PE=1 SV=2 (sp\|P92939\|ECA1_ARATH) | sp\|P92939\|ECA1_ARATH [2] | 0.028 | 0.6 | 58 | 67 | 45 | 47 | 34 | 24 | 44 | 39 |
| Alpha-soluble NSF attachment protein 2 OS=Arabidopsis thaliana GN=ASNAP2 PE=1 SV=1 | sp\|Q9SPE6\|SNAA2_ARATH | 0.05 | 0.6 | 10 | 7 | 10 | 6 | 4 | 6 | 7 | 4 |
| Calreticulin-1 OS=Arabidopsis thaliana GN=CRT1 PE=1 SV=1 | sp\|O04151\|CALR1_ARATH | 0.029 | 0.7 | 58 | 62 | 45 | 43 | 37 | 44 | 31 | 31 |
| Cluster of 60S ribosomal protein L30-2 OS=Arabidopsis thaliana GN=RPL30B PE=3 SV=1 (sp\|Q8VZ19\|RL302_ARATH) | sp\|Q8VZ19\|RL302_ARATH [2] | 0.048 | 0.7 | 8 | 8 | 10 | 10 | 6 | 5 | 4 | 9 |
| Cluster of Ras-related protein RABG3d OS=Arabidopsis thaliana GN=RABG3D PE=2 SV=1 (sp\|Q9C820\|RAG3D_ARATH) | sp\|Q9C820\|RAG3D_ARATH [2] | 0.038 | 0.8 | 26 | 31 | 22 | 22 | 20 | 21 | 17 | 19 |
| Patellin-3 OS=Arabidopsis thaliana GN=PATL3 PE=1 SV=2 | sp\|Q56Z59\|PATL3_ARATH | 0.029 | 1.3 | 29 | 39 | 29 | 26 | 39 | 36 | 44 | 45 |
| Cluster of Calcium-transporting ATPase 8, plasma membrane-type OS=Arabidopsis thaliana GN=ACA8 PE=1 SV=1 (sp\|Q9LF79\|ACA8_ARATH) | sp\|Q9LF79\|ACA8_ARATH [2] | 0.047 | 1.4 | 14 | 13 | 20 | 13 | 24 | 17 | 19 | 24 |
| GEM-like protein 1 OS=Arabidopsis thaliana GN=FIP1 PE=1 SV=1 | sp\|Q9SE96\|GEML1_ARATH | 0.044 | 1.5 | 6 | 4 | 6 | 4 | 9 | 9 | 6 | 6 |
| Cyclase-associated protein 1 OS=Arabidopsis thaliana GN=CAP1 PE=2 SV=1 | sp\|O65902\|ACAP1_ARATH | 0.032 | 1.6 | 3 | 4 | 4 | 4 | 4 | 6 | 7 | 6 |
| Probable plastid-lipid-associated protein 3, chloroplastic OS=Arabidopsis thaliana GN=PAP3 PE=2 SV=1 | sp\|O82291\|PAP3_ARATH | 0.038 | 1.6 | 4 | 4 | 3 | 3 | 4 | 6 | 6 | 5 |
| Acetyl-coenzyme A carboxylase carboxyl transferase subunit alpha, chloroplastic OS=Arabidopsis thaliana GN=CAC3 PE=1 SV=1 | sp\|Q9LD43\|ACCA_ARATH | 0.0054 | 1.7 | 11 | 14 | 10 | 11 | 16 | 23 | 17 | 21 |
| Cluster of Photosystem Q(B) protein OS=Gossypium barbadense GN=psbA PE=3 SV=1 (sp\|A0ZZ15\|PSBA_GOSBA) | sp\|A0ZZ15\|PSBA_GOSBA [52] | 0.014 | 1.8 | 2 | 1 | 3 | 1 | 3 | 4 | 3 | 4 |
| Ethanolamine-phosphate cytidylyltransferase OS=Arabidopsis thaliana GN=PECT1 PE=1 SV=1 | sp\|Q9ZVI9\|PECT1_ARATH | 0.016 | 1.8 | 2 | 4 | 6 | 5 | 6 | 8 | 9 | 8 |
| Cluster of 40S ribosomal protein S10-3 OS=Arabidopsis thaliana GN=RPS10C PE=2 SV=2 (sp\|Q9LTF2\|RS103_ARATH) | sp\|Q9LTF2\|RS103_ARATH [2] | 0.043 | 1.8 | 5 | 10 | 4 | 5 | 9 | 14 | 13 | 8 |
| Probable plastid-lipid-associated protein 2, chloroplastic OS=Arabidopsis thaliana GN=PAP2 PE=2 SV=1 | sp\|O49629\|PAP2_ARATH | 0.0088 | 1.9 | 3 | 4 | 4 | 1 | 5 | 6 | 5 | 6 |
| Lipoxygenase 6, chloroplastic OS=Arabidopsis thaliana GN=LOX6 PE=2 SV=1 | sp\|Q9CAG3\|LOX6_ARATH | 0.023 | 1.9 | 5 | 6 | 7 | 4 | 10 | 8 | 15 | 11 |
| Cluster of Histone H4 OS=Glycine max PE=3 SV=1 (sp\|P0CG89\|H4_SOYBN) | sp\|P0CG89\|H4_SOYBN [14] | 0.0025 | 2.1 | 2 | 1 | 3 | 2 | 5 | 5 | 4 | 4 |
| Beta-D-xylosidase 1 OS=Arabidopsis thaliana GN=BXL1 PE=1 SV=1 | sp\|Q9FGY1\|BXL1_ARATH | 0.0028 | 2.1 | 7 | 4 | 7 | 9 | 12 | 12 | 15 | 16 |
| Cluster of Alanine--tRNA ligase OS=Arabidopsis thaliana GN=ALATS PE=1 SV=3 (sp\|P36428\|SYA_ARATH) | sp\|P36428\|SYA_ARATH [4] | 0.019 | 2.2 | 8 | 8 | 9 | 6 | 13 | 18 | 27 | 14 |
| Probable protein phosphatase 2C 76 OS=Arabidopsis thaliana GN=At5g53140 PE=2 SV=1 | sp\|Q94AT1\|P2C76_ARATH | 0.037 | 2.2 | 1 | 0 | 1 | 1 | 2 | 1 | 2 | 1 |
| Pyruvate decarboxylase 2 OS=Arabidopsis thaliana GN=PDC2 PE=1 SV=1 | sp\|Q9FFT4\|PDC2_ARATH | 0.037 | 2.2 | 1 | 0 | 1 | 1 | 2 | 1 | 2 | 1 |
| Gamma carbonic anhydrase 1, mitochondrial OS=Arabidopsis thaliana GN=GAMMACA1 PE=1 SV=1 | sp\|Q9FWR5\|GCA1_ARATH | 0.04 | 2.3 | 2 | 0 | 2 | 2 | 4 | 2 | 3 | 5 |
| 40S ribosomal protein S29 OS=Arabidopsis thaliana GN=RPS29A PE=3 SV=2 | sp\|Q680P8\|RS29_ARATH | 0.027 | 2.4 | 1 | 0 | 1 | 1 | 2 | 2 | 1 | 2 |

| | | | | | | | | | | | |
|---|---|---|---|---|---|---|---|---|---|---|---|
| Probable plastid-lipid-associated protein 1, chloroplastic OS=Arabidopsis thaliana GN=PAP1 PE=1 SV=1 | sp\|O81439\|PAP1_ARATH | 0.029 | 2.4 | 3 | 2 | 2 | 1 | 3 | 6 | 4 | 7 |
| Cluster of DEAD-box ATP-dependent RNA helicase 2 OS=Arabidopsis thaliana GN=RH2 PE=2 SV=2 (sp\|Q94A52\|RH2_ARATH) | sp\|Q94A52\|RH2_ARATH [2] | 0.042 | 2.4 | 3 | 2 | 5 | 3 | 5 | 9 | 13 | 6 |
| Asparagine synthetase [glutamine-hydrolyzing] 2 OS=Arabidopsis thaliana GN=ASN2 PE=1 SV=1 | sp\|Q9LV77\|ASNS2_ARATH | 0.041 | 2.8 | 0 | 0 | 1 | 1 | 2 | 1 | 1 | 1 |
| Spermidine synthase 1 OS=Arabidopsis thaliana GN=SPDSYN1 PE=1 SV=1 | sp\|Q9ZUB3\|SPD1_ARATH | 0.042 | 3 | 1 | 0 | 0 | 1 | 2 | 2 | 1 | 1 |
| Probable LRR receptor-like serine/threonine-protein kinase MEE39 OS=Arabidopsis thaliana GN=MEE39 PE=2 SV=1 | sp\|C0LGP2\|MEE39_ARATH | 0.002 | 3.1 | 1 | 0 | 1 | 1 | 3 | 3 | 2 | 2 |
| Bifunctional aspartate aminotransferase and glutamate/aspartate-prephenate aminotransferase OS=Arabidopsis thaliana GN=PAT PE=1 SV=2 | sp\|Q9SIE1\|PAT_ARATH | 0.022 | 3.1 | 1 | 0 | 1 | 2 | 4 | 4 | 2 | 2 |
| Beta-glucosidase 46 OS=Arabidopsis thaliana GN=BGLU46 PE=1 SV=2 | sp\|O80690\|BGL46_ARATH | 0.035 | 3.2 | 0 | 0 | 1 | 1 | 2 | 2 | 1 | 1 |
| Xyloglucan endotransglucosylase/hydrolase protein 24 OS=Arabidopsis thaliana GN=XTH24 PE=1 SV=2 | sp\|P24806\|XTH24_ARATH | 0.032 | 3.3 | 2 | 0 | 1 | 7 | 9 | 6 | 13 | 7 |
| Phospholipase D beta 1 OS=Arabidopsis thaliana GN=PLDBETA1 PE=2 SV=4 | sp\|P93733\|PLDB1_ARATH | 0.041 | 3.4 | 1 | 1 | 2 | 0 | 4 | 4 | 5 | 1 |
| Cluster of Acetyl-CoA carboxylase 1 OS=Arabidopsis thaliana GN=ACC1 PE=1 SV=1 (sp\|Q38970\|ACC1_ARATH) | sp\|Q38970\|ACC1_ARATH [2] | 0.0061 | 3.5 | 2 | 0 | 2 | 2 | 4 | 4 | 6 | 7 |
| Cluster of Ribulose bisphosphate carboxylase large chain (Fragment) OS=Lavandula lanata GN=rbcL PE=3 SV=1 (sp\|Q33600\|RBL_LAVLA) | sp\|Q33600\|RBL_LAVLA [12] | 0.021 | 3.6 | 3 | 0 | 1 | 1 | 3 | 4 | 6 | 6 |
| Aspartate aminotransferase, mitochondrial OS=Arabidopsis thaliana GN=ASP1 PE=2 SV=1 | sp\|P46643\|AAT1_ARATH | 0.034 | 3.8 | 3 | 1 | 3 | 1 | 8 | 14 | 5 | 5 |
| Probable plastid-lipid-associated protein 9, chloroplastic OS=Arabidopsis thaliana GN=PAP9 PE=2 SV=1 | sp\|Q9M2P7\|PAP9_ARATH | 0.0059 | 3.9 | 0 | 0 | 1 | 1 | 2 | 1 | 2 | 2 |
| Mitochondrial carnitine/acylcarnitine carrier-like protein OS=Arabidopsis thaliana GN=BOU PE=2 SV=1 | sp\|Q93XM7\|MCAT_ARATH | 0.015 | 4 | 0 | 0 | 1 | 1 | 2 | 3 | 2 | 1 |
| Cluster of Ribulose bisphosphate carboxylase/oxygenase activase, chloroplastic OS=Arabidopsis thaliana GN=RCA PE=1 SV=2 (sp\|P10896\|RCA_ARATH) | sp\|P10896\|RCA_ARATH [3] | 0.019 | 4 | 1 | 0 | 0 | 2 | 4 | 4 | 2 | 2 |
| NADH dehydrogenase [ubiquinone] 1 beta subcomplex subunit 7 OS=Arabidopsis thaliana GN=At2g02050 PE=3 SV=1 | sp\|Q9SKC9\|NDUB7_ARATH | 0.021 | 4.3 | 0 | 0 | 0 | 1 | 1 | 1 | 1 | 1 |
| 3-oxoacyl-[acyl-carrier-protein] synthase III, chloroplastic OS=Arabidopsis thaliana GN=At1g62640 PE=2 SV=2 | sp\|P49243\|FABH_ARATH | 0.021 | 4.3 | 0 | 0 | 0 | 1 | 1 | 1 | 1 | 1 |
| Peroxiredoxin-2B OS=Arabidopsis thaliana GN=PRXIIB PE=1 SV=1 | sp\|Q9XEX2\|PRX2B_ARATH | 0.04 | 4.4 | 0 | 0 | 2 | 0 | 1 | 3 | 2 | 2 |
| RING-H2 finger protein ATL8 OS=Arabidopsis thaliana GN=ATL8 PE=2 SV=2 | sp\|Q8LC69\|ATL8_ARATH | 0.02 | 5.3 | 0 | 0 | 0 | 1 | 1 | 1 | 2 | 1 |
| Geminivirus Rep-interacting motor protein OS=Arabidopsis thaliana GN=GRIMP PE=1 SV=1 | sp\|Q9LX99\|GRIMP_ARATH | 0.028 | 5.5 | 1 | 0 | 0 | 0 | 1 | 1 | 1 | 2 |
| 3-isopropylmalate dehydratase small subunit 3 OS=Arabidopsis thaliana GN=At2g43090 PE=1 SV=1 | sp\|Q9ZW85\|LEUD3_ARATH | 0.0093 | 6.8 | 0 | 0 | 1 | 0 | 2 | 2 | 1 | 1 |
| RuvB-like protein 1 OS=Arabidopsis thaliana GN=RIN1 PE=1 SV=1 | sp\|Q9FMR9\|RIN1_ARATH | 0.042 | 7.5 | 0 | 0 | 1 | 0 | 2 | 1 | 3 | 1 |
| Cluster of Pectinesterase/pectinesterase inhibitor 3 OS=Arabidopsis thaliana GN=PME3 PE=2 SV=2 (sp\|O49006\|PME3_ARATH) | sp\|O49006\|PME3_ARATH [4] | 0.00027 | 9.1 | 0 | 0 | 1 | 0 | 2 | 2 | 2 | 2 |
| Phospholipase A I OS=Arabidopsis thaliana GN=PLA1 PE=2 SV=1 | sp\|F4HX15\|LPAI_ARATH | 0.023 | 9.2 | 1 | 0 | 0 | 0 | 4 | 1 | 3 | 1 |
| Probable galactinol--sucrose galactosyltransferase 6 OS=Arabidopsis thaliana GN=RFS6 PE=2 SV=2 | sp\|Q8RX87\|RFS6_ARATH | 0.0015 | 9.3 | 1 | 0 | 4 | 3 | 20 | 17 | 26 | 12 |
| Patellin-5 OS=Arabidopsis thaliana GN=PATL5 PE=1 SV=2 | sp\|Q9M0R2\|PATL5_ARATH | 0.0002 | ND | 0 | 0 | 0 | 0 | 2 | 2 | 2 | 1 |
| Glutathione synthetase, chloroplastic OS=Arabidopsis thaliana GN=GSH2 PE=2 SV=3 | sp\|P46416\|GSHB_ARATH | 0.0029 | ND | 0 | 0 | 0 | 0 | 2 | 1 | 1 | 1 |
| Protein TIC 20-II, chloroplastic OS=Arabidopsis thaliana GN=TIC20-II PE=2 SV=1 | sp\|O82251\|TI202_ARATH | 0.027 | ND | 0 | 0 | 0 | 0 | 0 | 1 | 1 | 1 |
| Adenine phosphoribosyltransferase 2 OS=Arabidopsis thaliana GN=APT2 PE=2 SV=1 | sp\|Q42563\|APT2_ARATH | 0.029 | ND | 0 | 0 | 0 | 0 | 2 | 1 | 2 | 0 |
| Uncharacterized aarF domain-containing protein kinase At5g05200, chloroplastic OS=Arabidopsis thaliana GN=At5g05200 PE=2 SV=1 | sp\|Q9ASX5\|Y5520_ARATH | 0.03 | ND | 0 | 0 | 0 | 0 | 1 | 1 | 1 | 0 |
| NADH dehydrogenase [ubiquinone] 1 beta subcomplex subunit 10-B OS=Arabidopsis thaliana GN=At3g18410 PE=2 SV=1 | sp\|Q94C12\|NDBAB_ARATH | 0.03 | ND | 0 | 0 | 0 | 0 | 1 | 1 | 1 | 0 |

free-GFP IP profile

| | | | | MS2 spectra count | | | | | | | |
|---|---|---|---|---|---|---|---|---|---|---|---|
| Description | Accession Number | t-test (p-value) | Fold Change by Category (Infected/mock) | free-GFP_m_1 | free-GFP_m_2 | free-GFP_m_3 | free-GFP_m_4 | free-GFP_i_1 | free-GFP_i_2 | free-GFP_i_3 | free-GFP_i_4 |
| Dolichyl-diphosphooligosaccharide--protein glycosyltransferase subunit STT3A OS=Arabidopsis thaliana GN=STT3A PE=2 SV=1 | sp\|Q93ZY3\|STT3A_ARATH | 0.029 | | 0 | 1 | 2 | 2 | 0 | 0 | 0 | 0 | 0 |
| Cluster of Putative calcium-transporting ATPase 11, plasma membrane-type OS=Arabidopsis thaliana GN=ACA11 PE=1 SV=1 (sp\|Q9M2L4\|ACA11_ARATH) | sp\|Q9M2L4\|ACA11_ARATH [2] | 0.046 | | 0 | 3 | 1 | 0 | 1 | 0 | 0 | 0 | 0 |
| Developmentally-regulated G-protein 3 OS=Arabidopsis thaliana GN=DRG3 PE=1 SV=1 | sp\|Q9SVA6\|DRG3_ARATH | 0.013 | | 0 | 1 | 1 | 1 | 2 | 0 | 0 | 0 | 0 |
| Cluster of Bifunctional aspartate aminotransferase and glutamate/aspartate-prephenate aminotransferase OS=Arabidopsis thaliana GN=PAT PE=1 SV=2 (sp\|Q9SIE1\|PAT_ARATH) | sp\|Q9SIE1\|PAT_ARATH [2] | 0.038 | | 0 | 3 | 0 | 2 | 1 | 0 | 0 | 0 | 0 |
| Myosin-17 OS=Arabidopsis thaliana GN=XI-K PE=1 SV=2 | sp\|F4K5J1\|MYO17_ARATH | 0.021 | | 0 | 3 | 1 | 1 | 1 | 0 | 0 | 0 | 0 |
| Cluster of Soluble inorganic pyrophosphatase 2 OS=Arabidopsis thaliana GN=PPA2 PE=2 SV=2 (sp\|P21216\|IPYR2_ARATH) | sp\|P21216\|IPYR2_ARATH [3] | 0.022 | | 0 | 3 | 1 | 1 | 1 | 0 | 0 | 0 | 0 |
| H/ACA ribonucleoprotein complex subunit 4 OS=Arabidopsis thaliana GN=CBF5 PE=1 SV=1 | sp\|Q9LD90\|CBF5_ARATH | 0.044 | | 0 | 3 | 1 | 1 | 1 | 0 | 0 | 0 | 0 |
| Cluster of Glucose-6-phosphate 1-dehydrogenase, cytoplasmic isoform 2 OS=Arabidopsis thaliana GN=ACG12 PE=2 SV=1 (sp\|Q9FJI5\|G6PD6_ARATH) | sp\|Q9FJI5\|G6PD6_ARATH [2] | 0.022 | | 0 | 3 | 1 | 2 | 1 | 0 | 0 | 0 | 0 |
| Protein RER1A OS=Arabidopsis thaliana GN=RER1A PE=1 SV=1 | sp\|O48670\|RER1A_ARATH | 0.016 | | 0 | 3 | 2 | 1 | 1 | 0 | 0 | 0 | 0 |
| Coatomer subunit beta-2 OS=Arabidopsis thaliana GN=At4g31490 PE=2 SV=2 | sp\|Q9SV20\|COPB2_ARATH (+1) | 0.02 | | 0 | 3 | 1 | 1 | 2 | 0 | 0 | 0 | 0 |
| Annexin D4 OS=Arabidopsis thaliana GN=ANN4 PE=2 SV=1 | sp\|Q9ZVJ6\|ANXD4_ARATH | 0.044 | | 0 | 3 | 1 | 0 | 3 | 0 | 0 | 0 | 0 |
| Cluster of Calcium-transporting ATPase 1, endoplasmic reticulum-type OS=Arabidopsis thaliana GN=ECA1 PE=1 SV=2 (sp\|P92939\|ECA1_ARATH) | sp\|P92939\|ECA1_ARATH [2] | 0.00053 | | 0 | 3 | 3 | 2 | 1 | 0 | 0 | 0 | 0 |
| Non-specific phospholipase C3 OS=Arabidopsis thaliana GN=NPC3 PE=2 SV=1 | sp\|Q9SRQ6\|NPC3_ARATH | 0.0057 | | 0 | 3 | 3 | 2 | 1 | 0 | 0 | 0 | 0 |
| Protein disulfide isomerase-like 1-4 OS=Arabidopsis thaliana GN=PDIL1-4 PE=1 SV=1 | sp\|Q9FF55\|PDI14_ARATH | 0.036 | | 0 | 3 | 4 | 0 | 2 | 0 | 0 | 0 | 0 |
| Polyadenylate-binding protein RBP45B OS=Arabidopsis thaliana GN=RBP45B PE=1 SV=1 | sp\|Q9SAB3\|RB45B_ARATH | 0.014 | | 0 | 4 | 2 | 1 | 2 | 0 | 0 | 0 | 0 |

**Appendix II. Label-free quantification of MEE39-GFP IP upon Fo5176 infection.**
The analysis from three (1-3) experiments of mock (m) and infected (i) samples are shown.

| | | | | LFQ intensity (a.u.) | | | | | | | | | | | |
|---|---|---|---|---|---|---|---|---|---|---|---|---|---|---|---|
| Name | AGI number | ANOVA p value | Significant pairs | MEE39_m_1 | MEE39_m_2 | MEE39_m_3 | MEE39_i_1 | MEE39_i_2 | MEE39_i_3 | Lti6B_m_1 | Lti6B_m_2 | Lti6B_m_3 | Lti6B_i_1 | Lti6B_i_2 | Lti6B_i_3 |
| Ribosomal protein L16p/L10e family protein | AT1G14320 | 0.0082983 | MEE39_i vs Lti6B_i | 24.8725 | 24.5984 | 23.6086 | 25.1565 | 25.9403 | 24.3695 | 24.2555 | 24.8417 | 0 | 0 | 0 | 0 |
| S18 ribosomal protein | AT1G22780; AT1G34030; AT4G09800 | 0.000504308 | MEE39_i vs Lti6B_i | 26.7774 | 27.5393 | 27.3347 | 27.5667 | 27.1137 | 27.3753 | 27.8165 | 27.934 | 26.6726 | 25.3926 | 24.4964 | 24.9804 |
| Ribosomal protein L22p/L17e family protein | AT1G27400 | 4.83E-12 | MEE39_i vs Lti6B_i | 24.3077 | 25.4234 | 24.6435 | 24.6331 | 25.4416 | 24.0699 | 24.4246 | 24.6045 | 24.5659 | 0 | 0 | 0 |
| Jacalin lectin family protein | AT1G33790 | 8.70E-10 | MEE39_i vs Lti6B_i | 27.245 | 27.8203 | 28.1788 | 27.1618 | 23.5967 | 25.508 | 27.5948 | 27.6808 | 26.9666 | 0 | 0 | 0 |
| choice-of-anchor C domain protein 2C putative (Protein of unknown function 2C DUF642) | AT1G80240 | 0.00628003 | MEE39_i vs Lti6B_i | 0 | 21.8731 | 22.2392 | 21.5674 | 23.0374 | 21.3167 | 0 | 0 | 0 | 0 | 0 | 0 |
| Ribosomal protein L18ae/LX family protein | AT2G34480 | 0.00885462 | MEE39_i vs Lti6B_i | 23.4998 | 24.1471 | 23.1017 | 24.852 | 24.5922 | 24.1818 | 23.9352 | 24.4101 | 0 | 0 | 0 | 0 |
| Ribosomal protein S5 family protein | AT2G41840 | 0.0065847 | MEE39_i vs Lti6B_i | 23.6181 | 24.2698 | 24.1575 | 23.8807 | 24.1066 | 24.689 | 24.4016 | 0 | 0 | 0 | 0 | 0 |
| Ribosomal protein S11 family protein | AT2G36160; AT3G11510 | 0.0119501 | MEE39_i vs Lti6B_i | 26.1268 | 27.4118 | 26.9652 | 26.4577 | 26.1737 | 26.9131 | 26.4901 | 26.7021 | 26.569 | 25.6912 | 25.3671 | 25.3519 |
| Ribosomal protein L13 family protein | AT3G24830 | 0.00875293 | MEE39_i vs Lti6B_i | 24.9437 | 24.7667 | 24.5083 | 25.605 | 25.792 | 24.6563 | 24.9961 | 25.2114 | 0 | 0 | 0 | 0 |
| MEE39, Leucine-rich repeat protein kinase family protein | AT3G46330 | 4.32E-12 | MEE39_i vs Lti6B_i; MEE39_m vs Lti6B_m | 30.7313 | 31.2323 | 31.5607 | 31.5828 | 32.2116 | 29.8411 | 0 | 0 | 0 | 0 | 0 | 0 |
| MIK2, Leucine-rich repeat receptor-like protein kinase family protein | AT4G08850 | 0.00409047 | MEE39_i vs Lti6B_i; MEE39_i vs MEE39_m | 0 | 20.6896 | 0 | 21.8766 | 22.9121 | 27.6643 | 0 | 0 | 0 | 0 | 0 | 0 |
| Ribosomal protein L23/L15e family protein | AT4G16720; AT4G17390 | 0.00813913 | MEE39_i vs Lti6B_i | 23.0431 | 22.9245 | 22.6448 | 23.5655 | 23.9098 | 23.3741 | 23.1694 | 22.8857 | 0 | 0 | 0 | 0 |
| Ribosomal protein S3Ae | AT4G34670 | 2.26E-11 | MEE39_i vs Lti6B_i | 24.375 | 25.7278 | 23.9886 | 25.3535 | 24.4643 | 24.853 | 24.8753 | 24.8036 | 24.1327 | 0 | 0 | 0 |
| Heavy metal transport/detoxification superfamily protein | AT4G35060 | 0.00564268 | MEE39_i vs Lti6B_i | 0 | 0 | 21.272 | 21.7031 | 21.9929 | 26.225 | 0 | 0 | 0 | 0 | 0 | 0 |
| Raffinose synthase family protein | AT5G20250 | 2.79E-07 | MEE39_i vs Lti6B_i; MEE39_i vs MEE39_m | 0 | 0 | 0 | 21.6381 | 22.9084 | 28.2754 | 0 | 0 | 0 | 0 | 0 | 0 |